

Regulation of nitrous oxide production in low oxygen waters off the coast of Peru

Claudia Frey^{1,2,*}, Hermann W. Bange², Eric P. Achterberg³, Amal Jayakumar¹, Carolin R. Löscher⁴, Damian L. Arévalo-Martínez², Elizabeth León-Palmero⁵, Mingshuang Sun², Xin Sun¹, Ruifang C. Xie³, Sergey Oleynik¹, Bess B. Ward¹

¹Department of Geoscience, Princeton University, Princeton, Guyot Hall, 08544 Princeton, USA

²Helmholtz Centre for Ocean Research Kiel, Düsternbrooker Weg 20, 24105 Kiel, Germany

³Helmholtz Centre for Ocean Research Kiel, Wischhofstr. 1-3, 24149 Kiel, Germany

⁴Department of Biology, Nordceee, Danish Institute for Advanced Study, University of Southern Denmark,

¹⁰⁵Departamento de Ecología, Facultad de Ciencias, Universidad de Granada, 18071, Granada, Spain

*current address: Department of Environmental Science, University of Basel, Bernoullistrasse 30, 4056 Basel, Switzerland

Keywords: ETSP, ODZ, denitrification, nitrification, N₂O production, ¹⁵N tracer incubations

15 Abstract. Oxygen deficient zones (ODZs) are major sites of net natural nitrous oxide (N₂O) production and emissions. In order to understand changes in the magnitude of N₂O production in response to global change, knowledge on the individual contributions of the major microbial pathways (nitrification and denitrification) to N₂O production and their regulation is needed. In the ODZ in the coastal area off Peru, the sensitivity of N₂O production to oxygen and organic matter was investigated using ¹⁵N-tracer experiments in combination with qPCR and microarray analysis of total and active functional genes targeting archaeal *amoA* and *nirS* as marker genes for nitrification and denitrification, respectively. Denitrification was responsible for the highest N₂O production with a mean of 8.7 nmol L⁻¹ d⁻¹ but up to 118 ± 27.8 nmol L⁻¹ d⁻¹ just below the oxic-anoxic interface. Highest N₂O production from ammonium oxidation (AO) of 0.16 ± 0.003 nmol L⁻¹ d⁻¹ occurred in the upper oxycline at O₂ concentrations of 10 - 30 µmol L⁻¹ which coincided with highest archaeal *amoA* transcripts/genes. Hybrid N₂O formation (i.e. N₂O with one N atom from NH₄⁺ and the other from other substrates such as NO₂⁻) was the dominant species, comprising 70 – 85 % of total produced N₂O from NH₄⁺, regardless of the ammonium oxidation rate or O₂ concentrations. Oxygen responses of N₂O production varied with substrate, but production and yields were generally highest below 10 µmol L⁻¹ O₂. Particulate organic matter additions increased N₂O production by denitrification up to 5-fold suggesting increased N₂O production during times of high particulate organic matter export. High N₂O yields of 2.1% from AO were measured, but the overall contribution by AO to N₂O production was still an order of magnitude lower than that of denitrification. Hence, these findings show that denitrification is the most important N₂O production process in low oxygen conditions fueled by organic carbon supply, which implies a positive feedback of the total oceanic N₂O sources in response to increasing oceanic deoxygenation.

35 **Introduction**

Nitrous oxide (N_2O) is a potent greenhouse gas (IPCC 2013) and precursor for nitric oxide (NO) radicals, which can catalyze the destruction of ozone in the stratosphere (Crutzen 1970, Johnston 1971), and is now the single most important ozone-depleting emission (Ravishankara et al. 2009). The ocean is a significant N_2O source, accounting for up to one third of all- natural emissions (IPCC 2013) and this source may increase substantially as 40 a result of eutrophication, warming, and ocean acidification (see e.g. Capone and Hutchins 2013, Breider et al. 2019). Major sites of oceanic N_2O emissions are regions with steep oxygen (O_2) gradients (oxycline), which are usually associated with coastal upwelling regions with high primary production at the surface. There, high microbial respiratory activity during organic matter decomposition leads to the formation of anoxic waters also 45 called oxygen deficient zones (ODZs), in which O_2 may decline to functionally anoxic conditions ($\text{O}_2 < 10 \text{ nmol kg}^{-1}$, Tiano et al. 2014). The most intense ODZs are found in the eastern tropical North Pacific (ETNP), the eastern tropical South Pacific (ETSP) and the northwestern Indian Ocean (Arabian Sea). The anoxic waters are surrounded by large volumes of hypoxic waters (below $20 \mu\text{mol L}^{-1} \text{O}_2$) which are strong net N_2O sources (Codispoti 2010; Babbin et al. 2015). Latest estimates of global, marine N_2O fluxes (Buitenhuis et al. 2018, Ji et al. 2018) agree 50 well with the 3.8 Tg N y^{-1} ($1.8 - 9.4 \text{ Tg N y}^{-1}$) reported by the IPCC (2013), but have large variability in the resolution on the regional scale, particularly along coasts where N_2O cycling is more dynamic. The expansion of 55 ODZs is predicted in global change scenarios and has already been documented in recent decades (Stramma et al. 2008, Schmidtko et al. 2017). This might lead to further intensification of marine N_2O emissions, which will constitute a positive feedback on global warming (Battaglia and Joos, 2018). However, decreasing N_2O emissions have also been predicted based on reduced nitrification rates due to reduced primary and export production (Martinez-Rey et al. 2015, Landolfi et al. 2017) and ocean acidification (Beman et al. 2011, Breider et al. 2019). The parametrization of N_2O production and consumption in global ocean models is crucial for realistic future 60 predictions, and therefore better understanding of their controlling mechanisms is needed.

N_2O can be produced by both nitrification and denitrification. Nitrification is a two-step process, comprising the oxidation of ammonia (NH_3) to nitrite (NO_2^-) (ammonia oxidation, AO) and NO_2^- to nitrate (NO_3^-) (65 NO_2^- oxidation). The relative contributions to AO by autotrophic ammonia-oxidizing archaea (AOA) and ammonia-oxidizing bacteria (AOB) have been inferred, based on the abundance of the archaeal and bacterial *amoA* genes, which encode subunit A of the key enzyme ammonia monooxygenase (e.g. (Francis et al. 2005, Mincer et al. 2007, Santoro et al. 2010, Wuchter et al. 2006)). These studies consistently revealed the dominance of archaeal over bacterial ammonia oxidizers, particularly in marine settings (Francis et al. 2005, Wuchter et al. 2006, Newell et al. 2011). In oxic conditions, AO by AOB and AOA forms N_2O as a by-product (Anderson 1964; Vajrala et al. 70 2013; Stein 2019) and AOA contribute significantly to N_2O production in the ocean (Santoro et al. 2011; Löscher et al. 2012). While hydroxylamine (NH_2OH) was long thought to be the only obligate intermediate in AO, NO has recently been identified as an obligate intermediate for AOB (Caranto and Lancaster 2017) and presumably AOA (Carini et al. 2018). Both intermediates are present in and around ODZs and correlated with nitrification activity 75 (Lutterbeck et al. 2018, Korth et al. 2019). Specific details about the precursor of NO to form N_2O in AOA remains controversial. Stieglemeier et al. (2014) concluded that NO is derived from NO_2^- reduction to form N_2O , while Carini et al. (2018) hypothesized that NO is derived from NH_2OH oxidation, which can then form N_2O . A hybrid N_2O production mechanism in AOA has been suggested, where NO from NO_2^- reacts with NH_2OH from NH_4^+ , which is thought to be abiotic, i.e., non-enzymatic (Koslovski et al. 2016). Abiotic N_2O production, also known as chemodenitrification, from intermediates like NH_2OH , NO or NO_2^- can occur under acidic conditions (Frame et

al. 2017), or in the presence of reduced metals like Fe or Mn and catalyzing surfaces (Zhu-Barker et al. 2015), but the evidence of abiotic N₂O production/chemodenitrification in ODZs is still lacking.

When O₂ concentrations fall below 20 $\mu\text{mol L}^{-1}$, nitrifiers produce N₂O from NO₂⁻, a process referred to as nitrifier - denitrification (Frame & Casciotti 2010), which has been observed in cultures of AOB (Frame & Casciotti 2010) and AOA (Santoro et al. 2011). During nitrifier-denitrification (and denitrification), two NO₂⁻ molecules form one N₂O, which thus differentiates this process from hybrid N₂O production. It has also been suggested that high concentration of organic particles create high NO₂⁻ and low-O₂ microenvironments enhancing nitrifier - denitrification (Charpentier et al. 2007). Overall, the yield of N₂O per NO₂⁻ generated from AO is lower in AOA than AOB (Hink et al. 2017a, 2017b) but it should be noted that the degree to which N₂O yield increases with decreasing O₂ concentrations varies with cell density in cultures and among field sites (Cohen & Gordon 1978; Yoshida 1988; Goreau et al. 1980; Frame & Casciotti 2010, Santoro et al. 2011, Löscher et al. 2012, Ji et al. 2015a, 2018a).

The anaerobic oxidation of ammonia by NO₂⁻ (anammox) to form N₂ is strictly anaerobic and important in the removal of fixed N from the system, but it is not known to contribute to N₂O production (Kartal et al. 2007, van der Star et al. 2008, Hu et al. 2019). In suboxic and O₂ free environments, oxidized nitrogen is respired by bacterial denitrification, which is the stepwise reduction of NO₃⁻ to elemental N₂ via NO₂⁻, NO and N₂O. N₂O as an intermediate can be consumed or produced, but at the core of the ODZ N₂O consumption through denitrification is enhanced, leading to an under saturation in this zone (Bange 2008, Kock et al. 2016). Reducing enzymes are highly regulated by O₂ concentrations and of the enzymes in the denitrification sequence, N₂O reductase is the most sensitive to O₂ (Zumft 1997), which can lead to the accumulation of N₂O along the upper and lower ODZ boundaries (Kock et al. 2016). N₂O accumulation during denitrification is mostly linked to O₂ inhibiting the N₂O reductase, but other factors such as sulfide accumulation (Dalsgaard et al. 2014), pH (Blum et al. 2018), high NO₃⁻ or NO₂⁻ concentrations (Ji et al. 2018), or copper limitation (Granger and Ward 2003) may also be relevant. Recent studies contrast the view of nitrification vs. denitrification as the main N₂O source in ODZs (Nicholls et al. 2007, Babbin et al. 2015, Ji et al. 2015a, Yang et al. 2017). They show the importance of denitrification in N₂O production in the ETNP from model outputs (Babbin et al. 2015) and in the ETSP from tracer incubation experiments (Dalsgaard et al. 2012, Ji et al. 2015a), based on natural abundance isotopes in N₂O (Casciotti et al. 2018) or from water mass analysis of apparent N₂O production ($\Delta\text{N}_2\text{O}$) and O₂ utilization (AOU) (Carrasco et al. 2017).^{45,46} N₂O production from the addition of ¹⁵N-labeled NH₄⁺, NO₂⁻ and/or NO₃⁻ revealed nitrification as a source of N₂O within the oxic-anoxic interface, but overall denitrification dominated N₂O production with higher rates at the interface and in anoxic waters (Ji et al. 2015a, 2018a). Denitrification is driven by organic matter exported from the photic zone and fuels blooms of denitrifiers leading to high N₂ production (Dalsgaard et al. 2012, Jayakumar et al. 2009, Babbin et al. 2014). Denitrification to N₂ is enhanced by organic matter additions and the degree of stimulation varies with quality and quantity of organic matter (Babbin et al. 2014). Because N₂O is an intermediate in denitrification, we hypothesize that its production should also be stimulated by organic matter, possibly leading to episodic and variable N₂O fluxes.

N₂O concentration profiles around ODZs appear to be at steady state (Babbin et al. 2015), but are much more variable in regions of intense coastal upwelling where high N₂O emissions can occur (Arévalo-Martínez et al. 2015). The contributions of and controls on the two N₂O production pathways under different conditions of O₂ and organic matter supply, are not well understood and may contribute to this variability. Hence, the goal of this study is to understand the factors regulating N₂O production around ODZs in order to better constrain how future

changes in O₂ concentration and carbon export will impact production, distribution and emissions of oceanic N₂O. Our goal was to determine the impact of O₂ and particulate organic matter on N₂O production rates using ¹⁵N tracer experiments in combination with qPCR and functional gene microarray analysis of the marker genes, *nirS* for 120 denitrification and *amoA* for AO by archaea, to assess how the abundance and structure of the community impacts N₂O production rates from the different pathways. ¹⁵N-labelled NH₄⁺ and NO₂⁻ was used to trace the production of single- (⁴⁵N₂O) and double- labelled (⁴⁶N₂O) N₂O to investigate the importance of hybrid N₂O production during AO along an O₂ gradient.

125 2 Materials and Methods

2.1 Sampling sites, sample collection and incubation experiments

130 Seawater was collected from 9 stations in the upwelling area off the coast of Peru in June 2017 onboard R/V Meteor (Figure 1). Water samples were collected from 10 L Niskin bottles on a rosette with a conductivity-temperature-depth profiler (CTD, seabird electronics 9plus system). In-situ O₂ concentrations (detection limit 2 μmol L⁻¹ O₂), temperature, pressure and salinity were recorded during each CTD cast. NO₂⁻ and NO₃⁻ concentrations were measured on board by standard spectrophotometric methods (Hydes et al. 2010) using a QuAAstro autoanalyzer (SEAL Analytical GmbH, Germany). NH₄⁺ concentrations were determined 135 fluorometrically using ortho- phthaldialdehyde according to Holmes et al. (1999). For N₂O, bubble-free triplicate samples were immediately sealed with butyl stoppers and aluminum crimps and fixed with 50 μL of saturated mercuric chloride (HgCl₂). A 10 mL He headspace was created and after an equilibration period of at least 2 hours 140 the headspace sample was measured with a gas chromatograph equipped with an electron capture detector (GC/ECD) according to Kock et al. (2016). The detection limit for N₂O concentration is 2nM ± 0.7nM. At all experimental depths nucleic acid samples were collected by filtering up to 5 L of seawater onto 0.2 μm pore size Sterivex-GP capsule filters (Millipore, Inc., Bedford, MA, USA). Immediately after collection filters were flash frozen in liquid nitrogen and kept at -80°C until extraction.

145 Three different experiments were carried out at coastal stations, continental slope and offshore stations. Experiments 1 and 2 aimed to investigate the influence of O₂ concentration along a natural and artificial O₂ gradient and experiment 3 targeted the impact of large particles (>50 μm) on N₂O production. Serum bottles were filled from the Niskin bottles with Tygon tubing after overflowing three times to minimize O₂ contamination. Bottles 150 were sealed bubble free with grey butyl rubber septa (National Scientific) and crimped with aluminum seals immediately after filling. The grey butyl rubber septa were boiled in MilliQ for 30min to degas and kept in a He atmosphere until usage. A 3 mL helium (He) headspace was created and samples from anoxic (O₂ < below detection) water depths were He purged for 15min. He purging removed dissolved oxygen contamination which is likely introduced during sampling and the headspace prevents possible oxygen leakage from the rubber seals 155 (DeBrabandere et al. 2012). Natural abundance 2000 ppb N₂O carrier gas (1000 μL in He) was injected to trap the produced labeled N₂O and to ensure a sufficient mass for isotope analysis. For all experiments, ¹⁵N-NO₂⁻, ¹⁵N-NO₃⁻, and ¹⁵N-NH₄⁺ tracer (¹⁵N/(¹⁴N+¹⁵N) = 99 atom-%) were injected into five bottles each from the same depth to a final concentration of 0.5 μmol L⁻¹, except for the NO₃⁻ incubations where 2 μmol L⁻¹ final concentration were anticipated to obtain 10 % label of the NO₃⁻ pool. The fraction labeled of the substrate pools was 0.76 – 0.99 for NH₄⁺, 0.11 – 0.99 for NO₂⁻, 0.055 – 0.11 for NO₃⁻. In the ¹⁵N-NO₃⁻ treatment, ¹⁴N-NO₂⁻ was added to trap the

label in the product pool for NO_3^- reduction rates and in the $^{15}\text{N}-\text{NH}_4^+$ treatment, $^{14}\text{N}-\text{NO}_2^-$ was added to a final concentration of $0.5 \mu\text{mol L}^{-1}$ to trap the label in the product pool for AO rates.

For the O_2 manipulation experiments, all serum bottles were He purged and after the addition of different amounts of air saturated site water a final headspace volume of 3 mL was achieved. Site water from the incubation 160 depth was shaken and exposed to air to reach full O_2 saturation. Then 0, 0.2, 0.5, 2 and 5mL O_2 saturated seawater was added into serum bottles and to reach final measured O_2 concentration of $0 \pm 0.18 \mu\text{M}$, $0.4 \pm 0.24 \mu\text{M}$, $1.6 \pm 0.12 \mu\text{M}$, $5.2 \pm 0.96 \mu\text{M}$ and $11.7 \pm 1.09 \mu\text{M}$ in seawater. For the $^{15}\text{N}-\text{NO}_3^-$ incubations two more O_2 treatments with 21.5 ± 2.8 and $30.2 \pm 3.35 \mu\text{M}$ O_2 were carried out to extend the range of a previous study in which N_2O production from $^{15}\text{NO}_3^-$ did not decrease in the presence of up to $7 \mu\text{M}$ O_2 (Ji et al. 2018). The O_2 concentration 165 was monitored with an O_2 sensor spot in one serum bottle per treatment using an O_2 probe and meter (FireSting, PyroScience, Aachen, Germany; Figure S1). The sensor spots are highly sensitive in the nanomolar range and prepared according to Larsen et al. (2016).

For the organic matter additions, concentrated particles $> 50 \mu\text{m}$ from 3 different depths were collected with a Challenger stand-alone pump system (SAPS *in situ* pumps, Liu et al. 2005), autoclaved and He purged. 170 200 μL of POC solution were added to each serum bottle before $^{15}\text{N}-\text{NO}_3^-$ or $^{14}\text{N}-\text{NO}_2^-$ tracer injection. The final particle concentrations and C/N ratios varied between $0.18 - 1.37 \mu\text{M C}$ and $8.1 - 15.4$, respectively (Table 2). The concentration and C/N ratio of PON and POC of the stock solutions were analyzed by mass spectrometry using GV Isoprime mass spectrometer.

A set of five bottles was incubated per time course. One bottle was sacrificed at t_0 , two bottles at t_1 and 175 two at t_2 to determine a single rate. Total incubation times were adjusted to prevent bottle effects, which become significant after 20 h based on respiration rate measurements (Tiano et al. 2014). Hence, experiments lasted from 12 hours (at the shelf stations) to 24 hours (at the slope stations). Incubation was terminated by adding 0.1 mL saturated mercuric chloride (HgCl_2). All samples were stored at room temperature in the dark and shipped back to the lab.

180

2.2 Isotope measurement and rate determination

The total N_2O in each incubation bottle was extracted with a purge-trap system according to Ji et al. (2015). Briefly, serum bottles were flushed with He for 35 min (38 ml min^{-1}), N_2O was trapped by liquid nitrogen, H_2O removed with an ethanol trap, a Nafion® trap and a $\text{Mg}(\text{ClO}_4)_2$ trap and CO_2 removed with an Ascarite CO_2 - 185 Adsorbance column and afterwards mass 44, 45, 46 and isotope ratios 45/44, 46/44 were detected with a GC-IRMS system (Delta V Plus, Thermo). Every two to three samples, a 20 mL glass vial with a known amount of N_2O gas was measured to calibrate for the N_2O concentration (linear correlation between N_2O peak size and concentration, $r^2 = 0.99$). The isotopic composition of the reference N_2O was $\delta^{15}\text{N} = 1.75 \pm 0.10 \text{ ‰}$ and $\delta^{18}\text{O} = 1.9 \pm 0.19 \text{ ‰}$ present in $^{15}\text{N}^{14}\text{N}^{16}\text{O}$ or $^{14}\text{N}^{15}\text{N}^{16}\text{O}$ for $^{45}\text{N}_2\text{O}$ and the less abundant $^{15}\text{N}^{15}\text{N}^{16}\text{O}$ for $^{46}\text{N}_2\text{O}$. To evaluate the 190 analyses of ^{15}N -enriched N_2O samples, internal isotope standards for $^{15}\text{N}_2\text{O}$ were prepared by mixing natural abundance KNO_3 of known $\delta^{15}\text{N}$ values with 99% $\text{Na}^{15}\text{NO}_3$ (Cambridge Isotope Laboratories) and converted to N_2O using the denitrifier method (Sigman et al. 2001, Weigand et al. 2016). Measured and expected values were compared based on a binomial distribution of ^{15}N and ^{14}N within the N_2O pool (Frame et al. 2017).

After N_2O analysis, samples incubated with $^{15}\text{NH}_4^+$ and $^{15}\text{NO}_3^-$ were analyzed for $^{15}\text{NO}_2^-$ to determine 195 rates of NH_4^+ oxidation and NO_3^- reduction, respectively. The individual sample size, adjusted to contain 20 nmol of N_2O , was transferred into 20 mL glass vials and He purged for 10 min. NO_2^- was converted to N_2O using sodium

azide in acetic acid (McIlvin and Altabet, 2005) and the nitrogen isotope ratio was measured on a Delta V Plus (Thermo).

For each serum bottle, total N₂O concentration (moles) and ⁴⁵N₂O/⁴⁴N₂O and ⁴⁶N₂O/⁴⁴N₂O ratios were converted to moles of ⁴⁴N₂O, ⁴⁵N₂O and ⁴⁶N₂O. N₂O production rates were calculated from the slope of the increase in mass 44, 45 and 46 over time (Figure S2). To quantify the pathways for N₂O production, rates were calculated based on the equations for N₂ production for denitrification and anammox (Thamdrup and Dalsgaard, 2002). In incubations with ¹⁵NH₄⁺ and unlabeled NO₂⁻, it is assumed that AO produces ⁴⁶N₂O from two labeled NH₄⁺ (equation 1) and some ⁴⁵N₂O-labeled N₂O based on binomial distribution (equation 2). If more single labelled N₂O is produced than expected (equation 2 and 3), a hybrid formation of one nitrogen atom from NH₄⁺ and one from NO₂⁻ (equation 4) is assumed to be taking place as found in archaeal ammonia oxidizers (Kozlowski et al. 2016). In incubations with ¹⁵NO₂⁻, we assume that ⁴⁶N₂O comes from nitrifier-denitrification or denitrification, which cannot be distinguished (equation 1). Hence, any production of ⁴⁵N₂O not attributed to denitrification stems from hybrid N₂O formation by archaeal nitrifiers (equation 4). In incubations with ¹⁵NO₃⁻, denitrification produces ⁴⁶N₂O and was the only process considered and hence was calculated based on equation (1). Rates (R) are calculated as nmol N₂O L⁻¹ d⁻¹ (Trimmer et al. 2016):

$$(1) R_{external} = slope^{46}N_2O \times (f_N)^{-2}$$

$$(2) R_{expected} = slope^{46}N_2O \times 2 \times (1 - f_N) \times (f_N)^{-1}$$

$$(3) R_{above} = slope^{45}N_2O - p^{45}N_2O_{expected}$$

$$(4) R_{hybrid} = (f_N)^{-1} \times (slope^{45}N_2O + 2 \times slope^{46}N_2O \times (1 - f_N^{-1}))$$

$$(5) R_{total} = pN_2O_{external} + pN_2O_{hybrid}$$

where f_N is the fraction of ¹⁵N in the substrate pool (NH₄⁺, NO₂⁻ or NO₃⁻), which is assumed to be constant over the incubation time. Hence, changing f_N due to any other concurrent N-consumption or production process during the incubation is neglected. Nevertheless, the assumption of constant f_N has implications that may affect the results. There is a potential for overestimating hybrid N₂O production in ¹⁵NO₂⁻ incubations by 5% in samples with high NO₃⁻ reduction rates. But in incubations from anoxic depths with high NO₃⁻ reduction rates, no hybrid N₂O production was found at all. For example, accounting for a decrease in f_N of the NO₃⁻ pool by active NO₂⁻ oxidation, the process with highest rates (Sun et al. 2017), had an effect of only $\pm 0.2\%$ on the final rate estimate. The presence of DNRA complicates ¹⁵N-labelling incubations because it can change f_N in all three tracer experiments. In ¹⁵NO₃⁻ incubations, active DNRA produces ¹⁵NO₂⁻ and ¹⁵NH₄⁺ from ¹⁵NO₃⁻, which can contribute to ⁴⁶N₂O production by AO. Even if a maximum DNRA rate (20 nM d⁻¹, Lam et al. 2009) is assumed to produce 0.02 nM ¹⁵NH₄⁺ during the 24 h incubations and all of it is oxidized (maximum N₂O production from AO 0.16 nM d⁻¹, this study) its contribution to ⁴⁶N₂O production is likely minor and within the standard error of the high N₂O production rates from NO₃. Hence an overestimation of the N₂O production rates is unlikely. The same applies in incubations with ¹⁵N-NO₂⁻ when DNRA produces ¹⁵NH₄⁺, additional ⁴⁶N₂O can be produced with a hybrid mechanism by AO. In ¹⁵NO₂⁻ incubations with high starting f_N (>0.7) the production of ¹⁴NO₂⁻ by NO₃⁻ reduction (which decreases f_N) leads to an underestimation by up to 9%, whereas in incubations with a low f_N (<0.3) the effect is less (up to 3% underestimation of N₂O production rates). In ¹⁵NH₄⁺ incubations (f_N >0.9), maximum DNRA rate would lead to an underestimation of 3.5%. Slope of ⁴⁶N₂O and slope of ⁴⁵N₂O represent the ⁴⁶N₂O and ⁴⁵N₂O production rates, which were tested for significance based on a linear regression (n=5, student t-test, R² >

0.80, p<0.05). Linear regressions that were not significantly different from zero were reported as 0. The error for each N₂O production rate was calculated as the standard error of the slope. Detection limits were 0.002 nmol L⁻¹ d⁻¹ for N₂O production from AO and 0.1 nmol L⁻¹ d⁻¹ for N₂O production from denitrification based on the average measured standard error for rates (Dalsgaard et al. 2012). The curve-fitting tool of Sigma Plot was used for the O₂ 240 sensitivity experiments. A one-way ANOVA was performed on the N₂O production rates to determine if rates were significantly different between POM treatments.

The rates (R) of NH₄⁺ oxidation to NO₂⁻ and NO₃⁻ reduction to NO₂⁻ were calculated based on the slope of the linear regression of ¹⁵NO₂⁻ enrichment over time (n = 5) (equation 6).

$$(6) \quad R = f_N^{-1} \times \text{slope} \delta^{15}\text{NO}_2^-$$

245 where f_N is the fraction of ¹⁵N in the substrate pool (NH₄⁺ or NO₃⁻).

Yield (%) of N₂O production during NH₄⁺ oxidation was defined as the ratio of the production rates (equation 7).

$$(7) \quad \text{Yield}_{\text{NH}4} = \frac{N - N_2\text{O}(\frac{nM}{d})}{N - \text{NO}_2^-(\frac{nM}{d})} \times 100\%$$

Yields of N₂O production during denitrification were calculated based on the fact that N₂O is not a side product during NO₃⁻ reduction to NO₂⁻ but rather the next intermediate during denitrification (equation 8).

$$250 \quad (8) \quad \text{Yield}_{\text{NO}3} = \frac{N - N_2\text{O}(\frac{nM}{d})}{N - \text{NO}_2^-(\frac{nM}{d}) + N - N_2\text{O}(\frac{nM}{d})} \times 100\%$$

All rates, yields and errors are reported in Table S3.

2.3 Molecular Analysis – qPCR, Microarrays

255 DNA and RNA were extracted using the DNA/RNA ALLPrep Mini Kit (Qiagen) followed by immediate cDNA Synthesis from purified and DNA-cleaned RNA using a SuperScript III First Strand Synthesis System (Invitrogen). The PicoGreen dsDNA Quantification Kit (Invitrogen) was used for DNA quantification and Quant-iT OliGreen ssDNA Quantification Kit (life technologies) was used for cDNA quantification.

260 The abundances of total and active *nirS* and archaeal *amoA* communities were determined by quantitative PCR (qPCR) with assays based on SYBR Green staining according to methods described previously (Jayakumar et al. 2013, Peng et al. 2013). Primers nirS1F and nirS3R (Braker et al. 1998) were used to amplify a 260-bp conserved region within the *nirS* gene. The *nirS* primers are not specific for epsilon-proteobacteria (Murdock et al. 2017), but in previous metagenomes from the ETSP epsilon-proteobacteria where below 3-4 % of the reads or not found, except in very sulfidic, coastal stations (Stewart et al. 2011, Wright et al. 2012, Ganesh et al. 2012, Schunck et al. 2013, Kavelage et al. 2015). Primers Arch-amoAF and Arch- amoAR (Francis et al. 2005) were 265 used to quantify archaeal *amoA* abundance. A standard curve containing 6 serial dilutions of a plasmid with either an archaeal *amoA* fragment or a *nirS* fragment was used on respective assay plates. Assays were performed in a StratageneMx3000P qPCR cycler (Agilent Technologies) in triplicates of 20- 25ng DNA or cDNA, along with a no primer control and a no template control. Cycle thresholds (Ct values) were determined automatically and used to calculate the number of *nirS* or archaeal *amoA* copies in each reaction, which was then normalized to copies per milliliter of seawater (assuming 100% recovery). The detection limit was around 15 copies mL⁻¹ based on the Ct values of the no template control.

Microarray experiments were carried out to describe the community composition of the total and active *nirS* and archaeal *amoA* groups using the DNA and cDNA qPCR products. Pooled qPCR triplicates were purified and cleaned using the QIAquick PCR Purification Kit (Qiagen). Microarray targets were prepared according to
275 Ward and Bouskill (2011). Briefly, dUaa was incorporated into DNA and cDNA targets during linear amplification with random octomers and a Klenow polymerase using the BioPrime kit (Invitrogen) and then labeled with Cy3, purified and quantified. Each probe is a 90-mer oligonucleotide consisting of a 70-mer archetype sequence combined with a 20-mer reference oligo as a control region bound to the glass slide. Each archetype probe represents a group of related sequences with $87 \pm 3\%$ sequence identity of the 70-mer sequence. Microarray targets
280 were hybridized in duplicates on a microarray slide, washed and scanned using a laser scanner 4200 (Agilent Technologies) and analyzed with GenePix Pro 6.0. The resulting fluorescence ratio (FR) of each archaeal *amoA* or *nirS* probe was divided by the FR of the maximum archaeal *amoA* or *nirS* FR on the same microarray to calculate the normalized FR (nFR). nFR represents the relative abundance of each archetype and was used for further analyses.

285 Two different arrays were used, BCO16 which contains 99 archaeal *amoA* archetype probes representing ~8000 archaeal *amoA* sequences (Biller et al. 2012) and BCO15 which contains 167 *nirS* archetype probes representing ~2000 sequences (collected from NCBI in 2009). A total of 74 assays were performed with 21 *nirS* cDNA targets, 21 *nirS* DNA targets, 16 *amoA* cDNA targets and 16 *amoA* DNA samples. The original microarray data from BCO15 and BCO16 are available via GEO (Gene Expression Omnibus; 290 <http://www.ncbi.nlm.nih.gov/geo/>) at NCBI (National Center for Biotechnology Information) under GEO Accession No GSE142806.

2.4. Data analysis

295 Spearman Rank correlation was performed from all N_2O production rates, AO and NO_3^- reduction rates, environmental variables, *nirS* and archaeal *amoA* gene and transcript abundance as well as the 20 most abundant archetypes of total and active *nirS* and *amoA* using R. Only significant values ($p < 0.05$) are shown. Archetype abundance (nFR) data were square-root transformed and beta-diversity was calculated with the Bray-Curtis coefficient. Alpha diversity of active and total *nirS* and *amoA* communities was estimated by calculating the Shannon diversity index using PRIMER6. Bray-Curtis dissimilarities were used to perform a Mantel test to determine significant differences between active and total communities of *nirS* and *amoA* using R (Version 3.0.2, 300 package “vegan” (Oksanen et al., 2019). Canonical Correspondence Analysis (CCA) (Legendre & Legendre 2012) was used to visualize differences in community composition dependent upon environmental conditions using the software PAST (Hammer et al. 2001). Before CCA analysis, a forward selection (Borcard et al. 1992) of the parameters that described the environmental and biological variables likely to explain the most significant part of the changes in the archetypes was performed.

305 The make.lefse command in MOTHUR was used to create a linear discriminant analysis (LDA) effect size (LEfSe) (Segata et al. 2011) input file from the MOTHUR shared file. This was followed by a LEfSe (<http://huttenhower.sph.harvard.edu/lefse/>) to test for discriminatory archetypes between O_2 levels. With a normalized relative abundance matrix, LEfSe uses the Kruskal-Wallis rank sum test to detect features with significantly different abundances between assigned archetypes in the different O_2 levels and performs an LDA to 310 estimate the effect size of each feature. A significant alpha of 0.05 and an effect size threshold of 2 were used for all marker genes discussed in this study.

3. Results

3.1 Hydrographic conditions

315 The upwelling system off Peru is a hot spot for N_2O emissions (Arévalo-Martínez et al. 2015) with most intense upwelling in austral winter but maximum chlorophyll during December to March (Chavez and Messié, 2009; Messié and Chavez, 2015). The sampling campaign took place during austral fall in the absence of intense upwelling or maximum chlorophyll. The focus of this study was the region close to the coast, which has highly variable N_2O concentration profiles (Kock et al. 2016) and N_2O emissions (Arévalo-Martínez et al. 2015). The
320 Peru Coastal Water (PCW, temperature <19.5°C, salinity 34.9 - 35.1) and the equatorial subsurface waters (ESSW, temperature 8-12°C, salinity 34.7 – 34.9) (Pietri et al. 2013) were the dominant water masses off the Peruvian coast sampled for N_2O production rate measurements (Table 1). At the southern-most transect at 15.5° – 16°S a meso-scale anticyclonic mode water eddy (McGillicuddy et al. 2007), which was about to detach from the coast, was detected from deepening/shoaling of the main/seasonal pycnoclines (Bange et al. 2018, Figure S3). Generally,
325 the stations were characterized by a thick anoxic layer (254 m – 427 m) reaching to the seafloor at two shelf stations (894, 883). NO_2^- concentration accumulated only up to 2 $\mu\text{mol L}^{-1}$ in the secondary NO_2^- maximum (SNM) at the northern transect (stations 882, 883), but up to 7.19 $\mu\text{mol L}^{-1}$ along the southern transect (Figure 2, station 907, 912). N_2O concentration profiles showed a high variability with respect to depth and O_2 concentrations (Figure 2). The southern transect (station 907, 912) showed the lowest N_2O concentrations (5 nmol L^{-1}) in the center
330 of the anoxic zones. At the same time, station 912 in the center of the eddy showed highest N_2O concentration with 78.9 nmol L^{-1} at $[\text{O}_2]$ below detection limit in the upper part of the anoxic zone. Above the ODZ, the maximum N_2O peak ranged from 57.9 – 78.9 nmol L^{-1} and was found at an O_2 concentration range from below detection (883, 894, 892, 912) up to 67 $\mu\text{mol L}^{-1}$ (907). Three stations (892, 894 and 904) showed high surface N_2O concentrations of 64 nmol L^{-1} .

335

3.2 Depth Distribution of N_2O production rates and total and active *nirS* and *amoA* abundance

340 N_2O production varied with depth and substrate (Figure 3, Table S3). In the oxycline, highest AO ($34 \pm 0.1 \text{ nmol L}^{-1} \text{ d}^{-1}$ and $35 \pm 9.2 \text{ nmol L}^{-1} \text{ d}^{-1}$) coincided with highest N_2O production from AO ($0.141 \pm 0.003 \text{ nmol L}^{-1} \text{ d}^{-1}$ and $0.159 \pm 0.003 \text{ nmol L}^{-1} \text{ d}^{-1}$) at both stations of the northern transect, stations 883 and 882, respectively (Figure 3(I)a, b). NH_4^+ oxidation and its N_2O production decreased to zero in the ODZ. The rates of the reductive source pathways for N_2O increased with depth. N_2O production from NO_2^- and NO_3^- displayed similar patterns with highest production at or below the oxic -anoxic interface (Figure 3(II)). N_2O production from NO_2^- showed highest rates of $3.06 \pm 1.17 \text{ nmol L}^{-1} \text{ d}^{-1}$ (912) and $2.37 \pm 0.54 \text{ nmol L}^{-1} \text{ d}^{-1}$ (906) further south (Figure 3(II) m, q) compared to lower rates at northern stations, where the maximum rate was $0.71 \pm 0.38 \text{ nmol L}^{-1} \text{ d}^{-1}$ (Figure 3(II) c, 883). A similar trend was found for N_2O production from NO_3^- : lower maximum rates at northern stations with $2.7 \pm 0.4 \text{ nmol L}^{-1} \text{ d}^{-1}$ (882) and $5.7 \pm 2.8 \text{ nmol L}^{-1} \text{ d}^{-1}$ (883, Figure 3(II) b) and highest rates in southern transects with $7.2 \pm 1.64 \text{ nmol L}^{-1} \text{ d}^{-1}$ ((Figure 3(II) l, 904) in transect 3 and up to $118.0 \pm 27.8 \text{ nmol L}^{-1} \text{ d}^{-1}$ (Figure 3(II) p, 912) in transect 4. Generally, N_2O production rates from NO_2^- and NO_3^- were 10 to 100-fold higher than from AO.

345 qPCR analysis detected lowest gene and transcript numbers of archaeal *amoA* and *nirS* in the surface mixed layer (Figure 3(I) k, l, 3(II)r, s). Highest archaeal *amoA* gene and transcript abundance was in the oxycline ($1 - 40 \mu\text{mol L}^{-1} \text{ O}_2$) with $24,500 \pm 340$ copies mL^{-1} and 626 ± 29 copies mL^{-1} at station 883 (Figure 3(I)c, d). *amoA* gene and transcript number decreased in the ODZ to $1000 - 6500$ gene copies mL^{-1} and 20 - 250 transcript

355 copies mL^{-1} . The profiles of *nirS* gene and transcript abundance were similar to each other (Figure 3(II) d, e) with highest abundance in the ODZ up to 1×10^6 copies mL^{-1} and 2.9×10^5 copies mL^{-1} , respectively. Denitrifier *nirS* genes and transcripts peaked in the anoxic layer and were significantly correlated with N_2O production from NO_2^- but not from NO_3^- . Archaeal *amoA* gene and transcript abundances were significantly correlated with AO and, N_2O production from AO (Figure S5). N_2O concentrations did not correlate with any of the measured variables (Figure S5).

360 3.3 Influence of O_2 concentration on N_2O production

365 N_2O production along the *in situ* O_2 gradient for the substrates NO_2^- and NO_3^- decreased exponentially with increasing O_2 concentrations (Figure 4b, c) while for NH_4^+ , the N_2O production was highest at highest sampled O_2 concentration (Figure 4a). At *in situ* O_2 levels above $8.4 \mu\text{mol L}^{-1}$ N_2O production decreased by 100% and 98% from NO_3^- and NO_2^- , respectively (Figure 4b, c).

370 In the manipulated O_2 treatments from the oxic - anoxic interface (S11, S19) a unimodal response of N_2O production from NH_4^+ and NO_2^- to O_2 is apparent (Figure 4d, e). Increasing and decreasing O_2 concentrations inhibited N_2O production from NH_4^+ and NO_2^- with the highest N_2O production rate between $1.4 - 6 \mu\text{mol O}_2 \text{ L}^{-1}$. However, this response was only significant in sample S11 (Figure 4d, e). There was no significant response to O_2 concentration of N_2O production from NO_3^- . O_2 did not inhibit N_2O production from NO_3^- up to $23 \mu\text{mol L}^{-1}$ (Figure 4f).

375 The proportion of hybrid N_2O produced during AO, i.e., the formation of N_2O from one $^{15}\text{NH}_4^+$ and one N compound (excluding NH_4^+) such as NO_2^- , NH_2OH or NO , was consistently between 70 – 85 % across different O_2 concentrations for manipulated and natural O_2 concentrations (Figure 5a, c). Hybrid formation during N_2O production from NO_2^- varied between 0 and 95% along the natural O_2 gradient (Figure 5b). In manipulated O_2 treatments hybrid formation from NO_2^- did not change across different O_2 treatments but with respect to the original depth, 0% in sample S11 which originated from 145 m of station 892 or 78% in sample S19 from 120m of station 894 (Figure 5d).

380 Highest N_2O yields during AO (over 1%) occurred between 1.4 and $2 \mu\text{mol O}_2 \text{ L}^{-1}$, and decreased at both higher and lower O_2 concentrations (Figure 6a). However, only the increase in yield from nmol O_2 to $1.4 - 2 \mu\text{mol L}^{-1} \text{ O}_2$ was significant (t-test, $p < 0.05$) and the following decrease in yield was not (t-test, $p > 0.05$). In the manipulated O_2 treatment of sample S19 (Figure 6c) the same significant pattern was observed, whereas in S11 highest yield was found at $12 \mu\text{mol L}^{-1} \text{ O}_2$. N_2O yield during NO_3^- reduction to NO_2^- decreased to zero at $8.4 \mu\text{mol L}^{-1} \text{ O}_2$ along the natural O_2 gradient (Figure 6b) while no significant response occurred in the manipulated O_2 treatments (Figure 6d). There, NO_3^- reduction was decreasing with increasing O_2 but N_2O production was steady 385 with increasing O_2 leading to high yields between $38.8 \pm 9\%$ - $91.2 \pm 47\%$ at $23 \mu\text{mol L}^{-1} \text{ O}_2$.

3.4 Effect of large particulate organic matter on N_2O production

390 The autoclaving of the concentrated POM solution liberated NH_4^+ from the particles, reducing the N/C ratio of the particles compared to non-autoclaved particles (Table 2). The highest NH_4^+ accumulation is found in samples with the largest difference in N/C ratios between autoclaved and non-autoclaved particles (Table 2, 904-20m, 898-100 m). Addition of $0.17 - 1.37 \mu\text{mol C L}^{-1}$ of autoclaved particles $> 50 \mu\text{m}$ (Table 2) produced a significant increase in N_2O production by up to 5.2- and 4.8-fold in 10 and 7 out of 19 additions for NO_2^- and NO_3^- respectively (Figure 7a, b). There was no linear correlation of the origin (mixed layer depth, oxycline or anoxic

zone), the quality (N/C ratio) or the quantity of the organic matter on the magnitude of the increase. Only samples 395 S20 and S17 were not stimulated by particle addition and N₂O production from denitrification did not significantly differ from the control (Figure 7b).

3.5 Diversity and community composition of total and active *nirS* and *amoA* assemblages and its correlation with environmental parameters

400 nFR values from functional gene microarrays were used to describe the nitrifier and denitrifier community composition of AOA and *nirS* assemblages, respectively. nFR was averaged from duplicate microarrays, which replicated well ($R^2 = 0.89 - 0.99$). Alpha- diversities of *nirS* and archaeal *amoA* were not statistically different for total and active communities (students t-test, $p > 0.05$), but were overall lower for RNA (3.2 ± 0.3) than DNA (3.8 ± 0.4) (Table S1). Principle Coordinate Analysis of Bray–Curtis similarity for each probe group on the microarray 405 indicated that the community structure of archaeal *amoA* genes was significantly different from that of archaeal *amoA* transcripts whereas community structure of *nirS* genes and transcripts did not differ significantly (Figure S4). To identify which archetypes were important in explaining differences in community structure of key 410 nitrification and denitrification genes, we identified archetypes that accounted for more than 1% of the total fluorescence for their probe set and that were significantly different with respect to ambient O₂ using a lefse analysis (Table S2). Furthermore, we used CCA to test whether the community composition, or even single archetypes, could explain the N₂O production rates.

415 The nFR distribution showed greater variability in the active (cDNA) AOA community than in the total community (DNA) among depths, stations and O₂ concentrations (Figure 8a, b). Archetypes over 1% made up between 76% (DNA) - 83% (cDNA) of the *amoA* assemblage and only 61% (DNA) - 68% (cDNA) of the *nirS* assemblage. The 4 most abundant AOA archetypes AOA55, AOA3, AOA21 and AOA32 made up 20% - 65% of the total and active community (Figure 8a, b). DNA of archetypes AOA55 and AOA79, both related to uncultured AOA in soils, significantly correlated with *in situ* NH₄⁺ concentrations (Figure S5). DNA and cDNA from AOA3 and AOA83 were significantly enriched in oxic waters and AOA7, closely related with crenarchaeote SCGC AAA288-M23 isolated from station ALOHA near Hawaii (Swan et al. 2011), was significantly enriched in anoxic 420 and hypoxic waters for DNA and cDNA respectively (Table S2). All other archetypes did not vary with O₂ levels. DNA of AOA 3, closely related to *Nitrosopelagicus brevis* (CN25), identified as the only archetype to be significantly correlated with N₂O production and yield from AO (Figure S5).

425 The total and active denitrifier communities were dominated by Nir7, derived from an uncultured clone from the ODZ in the ETSP (Lam et al. 2009), and Nir7 was significantly more enriched in the active community (Figure 8c, d). DNA from ODZ depths of the eddy, S15 (907, 130 m) and S17 (912, 90 m), diverged most obviously from the rest and from each other (Figure 8c, d). Interestingly, these two samples were not divergent among the active *nirS* community (Figure 8c, d; Figure S4). DNA of Nir35, belonging to the Flavobacteriaceae derived from coastal waters of the Arabian Sea (Goréguès et al., 2004), was most abundant (12.3 %) at the eddy edge (S15) as opposed to the eddy center (S17) where nir167, representing Anammox sequences from Peru, was most abundant 430 (12.0 %). Interestingly, Nir4 and Nir14, among the top 5 abundant archetypes, were significantly enriched in oxic water masses (Table S2). nFR signal of nir166, belonging to Scalindua, and Nir23 were among the top 5 abundant archetypes and significantly enriched in anoxic depths.

CCA is a direct gradient analysis, where the gradient in environmental variables is known a priori and the archetypes are considered to be a response to this gradient. Composition from total and active AOA community

435 did not differ between stations and all samples cluster close together (Figure S6a, b). S18 (912, 5 m) is a surface sample with lowest NO_3^- concentration ($8 \mu\text{mol L}^{-1}$), highest temperature and salinity of the data set and the DNA is positively related with O_2 and driven by AOA55, AOA32 and AOA79. RNA of S17 (912, 90 m) clusters with AOA70. AOA55 was abundant and its distribution is driven by O_2 and NH_4^+ (Figure S5).

440 CCA clustered the denitrifier community DNA into one main group with a few exceptions (Figure S6 c).
445 Two surface samples (S16, S18) clustered separate and were positively correlated with Nir4 and Nir14 and O_2 . Two anoxic samples from the eddy core (S17) and eddy edge (S15) clustered separate with S17 being driven by 3 *nirS* archetypes – Nir54, Nir10 and Nir167 and S15 by Nir23, Nir35 and Nir133 (Figure S6 c). Total and active *nirS* community composition did not differ as a function of O_2 . Although, composition of active and total *nirS* communities were not significantly different, the active community clustered slightly differently. For *nirS* RNA, surface and oxycline samples (S16 and S10) grouped together and were correlated positively with O_2 , temperature and salinity, whereas the anoxic eddy samples did not differ from the rest (Figure S6d). N_2O production from NO_2^- significantly correlated with *nirS* gene and transcript abundance but both reductive N_2O production pathways were not linked with a single dominant *nirS* archetype (Figure S5)

450 **4. Discussion**

Most samples originated from Peru Coastal Water (PCW) characterized by supersaturated N_2O concentrations (Kock et al. 2016, Bourbonnais et al. 2017). Only the deepest sample (S1, 882 - 350m) saw the presence of a different water mass, the equatorial subsurface waters. Thus, our findings about regulation of N_2O production at different stations probably apply to the region as a whole. Several studies indicate that water mass hydrography plays an important role in shaping microbial community diversity (Biller et al. 2012, Hamdan et al. 2012) and a coupling of *amoA* alpha diversity to physical conditions such as salinity, temperature and depth has been shown in coastal waters off Chile (Bertagnolli and Ulloa 2017). While salinity, temperature and depth were prominent factors in shaping the community compositions of nitrifiers and denitrifiers (Figure S6), for N_2O production rates correlations with physical and chemical parameters were not consistent. On one hand, oxidative N_2O production from NH_4^+ positively correlated with temperature, salinity, oxygen and negatively with depth and PO_4^{3-} concentration. On the other hand, reductive N_2O production from NO_2^- positively correlated with NH_4^+ and NO_2^- concentrations, but negatively with NO_3^- concentrations (Figure S5), suggesting when NO_3^- is abundant, denitrifiers are less likely to use NO_2^- for N_2O production during denitrification. Both oxidative (AO) and reductive (NO_2^- and NO_3^- reduction) N cycling processes produced N_2O with differential effects of O_2 on them. Measured N_2O production rates were always highest from NO_3^- , followed by NO_2^- and NH_4^+ , which is consistent with previous studies that showed denitrification as a dominant N_2O source in Peruvian coastal waters harboring an ODZ (Ji et al. 2015a, Casciotti et al. 2018). A low contribution of AO to N_2O production in low O_2 waters is in line with a previous study in this area estimating N_2O production based on isotopomer measurements combined with a 3-D Reaction-Advection-Diffusion Box model (Bourbonnais et al. 2017). The low percentage that AO contributed to total N_2O production was between 0.5 – 6%, with one exception in the shallowest sample S5 with $30 \mu\text{mol L}^{-1} \text{O}_2$ where AO contributed 86% to total N_2O production. We found strong positive effects of decreasing O_2 concentration and increasing particulate matter concentrations on N_2O production in the upper oxycline.

475 The occurrence of an anticyclonic mode water eddy at 16°S (transect 4, stations 912, 907) at the time of sampling was not unusual, as such eddies have been reported at a similar position (Stramma et al. 2013). High N loss, a large SNM with low NO_3^- concentrations and strong N_2O depletion in the core of ODZ of the eddy result

in reduced N₂O inside of this kind of eddies as they age and are advected westward (Cornejo D`Ottone et al. 2016, Arévalo-Martínez et al. 2016). Our study found similar patterns with largest SNM (5.23 μM NO₂⁻), lowest NO₃⁻ (14 $\mu\text{mol L}^{-1}$) and N₂O (4 nmol L⁻¹) concentrations in the eddy center. For the first time N₂O production rates were measured in an eddy, and the rates of up to $118 \pm 27 \text{ nmol L}^{-1} \text{ d}^{-1}$ are the highest N₂O production rates from 480 denitrification reported in the ETSP. Previously reported maximum rates were up to $86 \text{ nmol L}^{-1} \text{ d}^{-1}$ (Dalsgaard et al. 2012) based on ¹⁵N tracer incubations. Much smaller maximum rates, $49 \text{ nmol L}^{-1} \text{ d}^{-1}$ (Bourbonnais et al. 2017) and $50 \text{ nmol L}^{-1} \text{ d}^{-1}$ (Farías et al. 2009), were obtained using N₂O isotope and isotopomer approaches, which 485 provide time and process integrated signals. Hence, the deviation of maximum rates can be explained by 1) the different approaches and 2) the sampling of the core of the eddy. N₂ production measurements (from anammox and denitrification) were not performed in this study, but should be in future studies to account for potential artefacts by co-occurring NO₃⁻ reduction processes. Here, it cannot be determined whether the eddy only stimulated 490 N₂O production but not N₂ production from denitrification (i.e. increasing the N₂O/N₂ yield) or if the eddy also increased complete denitrification to N₂ by 10 times compared to stations outside of the eddy. Considering that at some depths only incomplete denitrification (also known as “stop- and go” denitrification) to N₂O is at work, it 495 would not be surprising that N₂O production can reach the same order of magnitude as N₂ production from complete denitrification. Aged eddies also show lower N₂O concentration maxima at the upper oxycline (Arévalo-Martínez et al. 2016), which was not the case in this study where a young eddy was just about to detach from the coast. In fact, the eddy stations show the highest N₂O peak in the upper oxycline within this data set. Eddies and 500 their age imprint mesoscale patchiness and heterogeneity in biogeochemical cycling. It appears that young eddies close to the coast with high N₂O concentrations and high N₂O production rates have a great potential for high N₂O emissions compared to aged eddies or waters surrounding eddies.

4.1 Effect of O₂ on reductive and oxidative N₂O production

The relationship between O₂ concentrations and N₂O production by nitrification and denitrification is 500 very complex in ODZs. While poorly constrained, the reported O₂ threshold level (1.7 $\mu\text{mol L}^{-1}$ O₂) for reductive N₂O production is lower (Dalsgaard et al. 2014) than the reported O₂ threshold level (8 $\mu\text{mol L}^{-1}$) for N₂O consumption in the ETSP (Cornejo and Farías 2012). Nevertheless, the suboxic zone between 1 – 8 $\mu\text{mol L}^{-1}$ O₂ carries high N₂O concentrations indicating higher N₂O production than consumption. In this study, we focused on 505 this suboxic water masses above the ODZ and determined bulk kinetics of O₂ sensitivity in batch experiments, which reflect the metabolism of the microbial community. The effect of O₂ on N₂O production differed between natural O₂ concentrations with varying communities vs. manipulated O₂ concentrations within a community. While N₂O production from NO₂⁻ and NO₃⁻ decreased exponentially along the natural O₂ gradient, it did not always decrease for the manipulated O₂ treatments. Unchanged N₂O production with higher O₂ levels in NO₃⁻ treatments showed that at least a portion of the community can respond very differently to a sudden increase in O₂ than 510 predicted from natural O₂ gradients with communities acclimated to a certain O₂ concentration. In the ETNP, this pattern has been observed before (Ji et al. 2018a) but the mechanism behind it is unknown. Different responses of N₂O production rates to O₂ between *in situ* assemblages and incubated samples were not unexpected because different rates at different depths were likely not only due to O₂ differences but also other factors such as different organic matter fluxes and different amounts and types of N₂O producers at different depths. In addition, sampling 515 with Niskin bottles and purging can induce stress responses (Stewart et al. 2012) and shift the richness and structure of the microbial community from the *in situ* community (Torres-Beltran et al. 2019). The removal of other gases

like H₂S during purging is another potential artefact. However, it is unlikely as measurable H₂S concentrations have mostly been found at very shallow coastal stations (< 100 m deep) (Callbeck et al. 2018), not the environment of this study. On the contrary, high abundances (up to 12%) of sulfur oxidizing gamma proteobacteria, like SUP05 520 can be found in eddy-transported offshore waters where they actively contributed to autotrophic denitrification (Calbeck et al. 2018). In this study, we cannot differentiate between autotrophic or organotrophic denitrification, but a contribution of autotrophic denitrification in the eddy center is likely. Off the Chilean coast, active N₂O production by denitrification was found at up to 50 $\mu\text{mol L}^{-1}$ O₂ (Farías et al. 2009). These results reinforce prior 525 studies showing that distinct steps of multistep metabolic pathways, such as denitrification, can differ in O₂ sensitivity (Dalsgaard et al. 2014, Bristow et al. 2016a, 2016b). In various bacterial strains and natural communities, the NO₃⁻ reductase enzyme (*Nar*) which catalyzes the first step in denitrification, is reportedly the most O₂ tolerant, followed by the more O₂ sensitive steps of NO₂⁻ reduction (*Nir*) and N₂O reduction (Körner und Zumft 1989, McKenney et al. 1994, Kalvelage et al. 2011). The fact that N₂O production is insensitive to 530 manipulated O₂ in the NO₃⁻ treatments and not in the NO₂⁻ treatments is evidence that it is not due to inhibition of the reduction of N₂O to N₂ at higher O₂ because then both treatments would look similar. It further indicates that high N₂O production from NO₃⁻ in high oxygen treatments is unlikely an effect of anoxic microniches. While 535 anoxic microniches in batch incubations can never be fully ruled out, there is no reason why they should systematically change N₂O production in NO₃⁻ from NO₂⁻ incubations at the same oxygen treatment. We suggest a stimulation of incomplete denitrification, which leads to the accumulation of N₂O in the serum bottles rather than a stimulation of overall denitrification rates to N₂. While NO₃⁻ reduction was inhibited by higher O₂ 540 concentrations, N₂O production was not, leading to very high yields of N₂O production per NO₂⁻ produced. We hypothesize that there is a direct channeling of reduced NO₃⁻ to N₂O without exchange of an internal NO₂⁻ pool with the surrounding NO₂⁻. Long turnover times for NO₂⁻ have been inferred from $\delta^{18}\text{O}$ of NO₂⁻, which was fully 545 equilibrated with water in the offshore waters (Bourbonnais et al. 2015) and more dynamic in the coastal waters (Hu et al. 2016) supporting our hypothesis. If NO₂⁻ does not exchange, our rate estimates for NO₃⁻ reduction based on produced ¹⁵N-NO₂⁻ are underestimated resulting in high yields. A low NO₂⁻ exchange rate has been shown before (Ji et al. 2018b). Based on the assumption that all labelled N₂O from ¹⁵NO₃⁻ has gone through the NO₂⁻ pool, we include the NO₂⁻ pool into calculating f_N. In ¹⁵NO₃⁻ incubations the enrichment of the substrate pool was low (f_N = 0.05 – 0.1) and including NO₂⁻ resulted in an underestimation of no more than 5 % depending on the *in situ* NO₂⁻ concentration, and thus does not explain the high rates.

One N₂O producing process not considered in this study is fungal denitrification, but it deserves mentioning because in soils and coastal sediments it contributes substantially to N₂O production (Wankel et al. 2017, Shoun et al. 2012). With ¹⁵N-labelling experiments it is not possible to distinguish between bacterial and fungal denitrification. In ODZs, marine fungal communities show a wide diversity (Jebaraj et al. 2012) and a high 550 adaptive capability is suggested (Richards et al. 2012). Most fungal denitrifiers lack the capability to reduce N₂O to N₂, hence all NO₃⁻ reduction results in N₂O production (Richards et al. 2012). In a culture study, the fungus, *Fusarium oxysporum*, needed O₂ exposure before it started to denitrify (Zhou et al. 2001). To what extent marine fungi play a role in denitrification in open ocean ODZs and their O₂ sensitivity remains to be investigated.

N₂O production from NH₄⁺ did not decrease exponentially with increasing O₂ as shown previously for 555 the ETSP (Qin et al. 2017, Ji et al. 2018a, Santoro et al. 2011). N₂O production rather increased with increasing *in situ* oxygen and had an optimum between 1.4 – 6 $\mu\text{mol O}_2 \text{ L}^{-1}$ in manipulated O₂ treatments. A similar optimum curve was observed in cultures of the marine AOA *Nitrosopumilus maritimus*, where N₂O production reached

maxima at O_2 concentrations between 2 - 10 $\mu\text{mol L}^{-1}$ (Hink et al. 2017a). Furthermore, N_2O production by *N. viennensis* and *N. maritimus* was not affected by O_2 but instead by the rate of AO (Stieglmeier et al. 2014, Hink et al. 2017a). To find out if this is the case in our study, we plotted AO rate against N_2O production from NH_4^+ for natural and manipulated O_2 samples (Figure S7). The resulting significant linear fit ($R^2 = 0.75$, $p < 0.0001$) implies that the rate of AO was the main driver for the intensity of N_2O production from NH_4^+ and oxygen had a secondary effect.

Discrepancies in estimates of the O_2 sensitivity of N_2O production by nitrification and denitrification are likely due to a combination of taxonomic variation as well as differences in sensitivity among the various enzymes of each pathway.

4.2 N_2O yields and hybrid N_2O formation from NH_4^+

N_2O yields of AO were 0.15 – 2.07 % ($N_2O\text{-N mol} / \text{NO}_2^-\text{-N mol} = 1.5 \times 10^{-3} – 20.7 \times 10^{-3}$) which are at the higher end of most marine AOA culture or field studies (Hink et al 2017b, Qin et al. 2017, Santoro et al. 2011, Stieglmeier et al. 2014). Only in 2015 off the coast of Peru a higher maximum yield of 3.14% was reported (Ji et al. 2018a). While high N_2O yields are usually found in low O_2 waters ($< 6 \mu\text{mol L}^{-1}$), in this study AO had also high yields at higher oxygen concentrations, 0.9 % at $30 \mu\text{mol L}^{-1} O_2$ compared to previous studies (0.06% at $> 50 \mu\text{mol L}^{-1}$ Ji et al. 2018a).. In near coastal regions, higher N_2O yield at higher O_2 concentrations expands the overall water volume where N_2O production by AO contributes to high N_2O concentration, which is more likely to be emitted to the atmosphere.

Insights into the production mechanism of N_2O is gained from hybrid- N_2O formation based on differentiating between production of single ($^{45}\text{N}_2O$) and double ($^{46}\text{N}_2O$) - labelled N_2O . If the production of $^{45}\text{N}_2O$ is higher than what is expected based on the binomial distribution, then an additional source of ^{14}N can be assumed. In $^{15}\text{NH}_4^+$ incubations, as potential ^{14}N substrates (besides NH_4^+), NO_2^- , NH_2OH and HNO are most likely. Even though, *in situ* NH_4^+ is below detection in almost all water depths ($f_N > 0.9$), there remains the potential for $^{15}\text{NH}_4^+$ pool dilution by remineralization and DNRA during the incubation. Studies have shown fast turnover for NH_4^+ , despite low NH_4^+ concentrations (e.g.. Klawonn et al. 2019). Even if hybrid N_2O production rates are overestimated, it remains the major N_2O production mechanisms from AO in this study. In future ^{15}N -labelling studies, co-occurrence of NH_4^+ production by DNRA or degradation should be measured along with N_2O production to account for pool dilution. Whether hybrid N_2O formation is purely abiotic, a mix of biotic and abiotic or biotic reactions, is debatable (Stieglmeier et al. 2014, Kozlowski et al. 2016, Carini et al. 2018, Lancaster et al. 2018, Stein 2019). Hybrid N_2O production from NO_2^- was variable with depth and oxygen, which can be explained by the different proportions of nitrifier versus denitrifier NO_2^- reduction to N_2O . For example, in the interface sample S19 (892, 144 m, $3.69 \mu\text{mol L}^{-1} \text{NO}_2^-$) N_2O production from NO_2^- ($0.72 \pm 0.19 \text{ nmol L}^{-1} \text{ d}^{-1}$) was 20 times higher than from NH_4^+ ($0.033 \pm 0.0004 \text{ nmol L}^{-1} \text{ d}^{-1}$) and no hybrid N_2O formation from NO_2^- was found (Figure 5d). There, the major N_2O production mechanism seems to be by denitrification rather than nitrification, and even if there was a hybrid production we were not able to detect it within the given error ranges. Hybrid N_2O production from NH_4^+ was independent of the rate at which N_2O production took place and independent of the O_2 concentration and varied little (70 – 86% of total N_2O production) during AO. Therefore, a purely abiotic reaction outside and without the vicinity of the cell can be excluded because concentrations of potential substrates for abiotic N_2O production like $\text{Fe}(\text{II})$, Mn , NO , NH_2OH vary with depth and O_2 concentration (Zhu-Barker et al. 2015, Kondo and Moffet 2015, Lutterbeck et al. 2018, Korth et al. 2019). Additionally, at four depths the potential

for abiotic N_2O production in $^{15}\text{NO}_2^-$ addition experiments showed variations with depth and no significant impact 600 of HgCl_2 fixation (Figure S9). Hence, any ^{14}N which is integrated into N_2O to produce a hybrid/single labelled N_2O has to be passively or actively taken up by the cell first (Figure 9). There, it reacts with an intermediate product (^{15}NO or $^{15}\text{NH}_2\text{OH}$) of AO inside the cell. With this set of experiments, it is not possible to disentangle if hybrid production is based on an enzymatic reaction or an abiotic reaction inside the cell. Caranto et al. (2017) 605 showed that the main substrate of NH_2OH oxidation is NO , making NO an obligate intermediate of AO in AOB and suggested the existence of an unknown enzyme that catalyzes NO oxidation to NO_2^- (further details also in Stein 2019). If NO is an obligate intermediate of AO in AOA (Lancaster et al. 2018), a constant rate of spontaneous 610 abiotic or enzymatic N_2O production is very likely, which always depends on the amount of NO produced in the first place. This could explain why we consistently find ~80% hybrid formation at high as well as at low AO rates. Further studies are needed to investigate the full mechanisms.

610

4.3 Effect of particulate organic matter on N_2O production

A positive stimulation of N_2O production from denitrification by particulate organic matter was found, 615 indicating carbon limitation of denitrification in the ETSP. The experimental POM amendments simulated a low POC export flux and represented a flux that happens over 2 - 15 days, assuming an export flux of $3.8 \text{ mmol m}^{-2} \text{ d}^{-1}$ and that 8% of the total POC pool is $>50 \mu\text{m}$ (Boyd et al. 1999, Martin et al. 1987, Haskell et al. 2015). We are 620 aware that the POM collected by *in situ* pumps is a mix of suspended and sinking particles and hence the flux should be considered a rough estimate. However, the particle size ($>50 \mu\text{m}$) used in the experiments is indicative of sinking particles. The stimulation of N_2 production from denitrification by particulate organic matter has been shown in ODZs before (Ward et al. 2008, Chang et al. 2014), with quantity and quality of organic matter 625 influencing the degree of stimulation (Babbin et al. 2014). In this study, amendments of POM at different degradation stages resulted in variable magnitudes of N_2O production from NO_2^- and NO_3^- with no significant correlations between magnitude of the rates and amount, origin or quality of POM added. The processing of the particles has reduced the original N/C ratios of POM from the mixed layer more than of the POM from the ODZ, 630 resulting in similar N/C ratios of particles from different depths. This could be one possible explanation for a lack of correlation of N_2O production with origin of the POM. Furthermore, N_2 production was not quantified and hence it is not possible to evaluate potential relationships between overall N loss and POM additions or whether 635 the partitioning between N_2O and N_2 varied among treatments and depths. $\text{N}_2\text{O}/\text{N}_2$ production ratio can vary from 0 - 100% (Dalsgaard et al. 2014, Bonaglia et al. 2016). A temporary accumulation of N_2O before further reduction to N_2 in the incubations can be ruled out as N_2O accumulated linearly over time. The only station, where POM 640 additions did not stimulate N_2O production was in the center of the young eddy (912-S17). There, the highest rates of N_2O production from NO_3^- ($118 \text{ nmol L}^{-1} \text{ d}^{-1}$) were found, indicating that denitrification was not carbon limited. This is consistent with previous studies on anti-cyclonic eddies, which have shown high N loss in the core of a 645 young eddy that weakened with aging of the eddy (Stramma et al. 2013, Bourbonnais et al. 2015, Löscher et al. 2016). A direct link between the freshly produced POM fueling N loss on one hand, and decreased N loss with aging due to POM export out of the eddy on the other hand, was proposed (Bourbonnais et al. 2015, Löscher et al. 650 2016). In this study, the young eddy is a hot spot for N_2O production.

Besides carbon availability as electron donor for denitrification, copper limitation and high NO_3^- availability may play a role. Copper limitation has been argued to lead to N_2O accumulation by inhibiting the copper-dependent N_2O reductase (Granger and Ward 2003, Bonaglia et al. 2016), but it was not a limiting factor

640 for denitrification in the three major ODZs previously (Ward et al. 2008). Water sampling from Niskin bottles in our study was not trace metal clean and could be contaminated with Copper from the sampling system, making a limitation of trace metals in our incubations unlikely. However, OM fueled N₂O production may have become limited by the availability of copper during the incubation.

645 High NO₃⁻ availability increases N₂O production from denitrification in salt marshes (Ji et al. 2015b) and in soils (Weier et al. 1993), systems which are generally not carbon limited. Also, at the oxic - anoxic interface of Chesapeake Bay, the ratio of NO₂⁻ to NO₃⁻ concentration was identified as a driver for high N₂O production from NO₃⁻ (Ji et al. 2018b). This study also found higher N₂O production rates from NO₃⁻ than NO₂⁻, which linearly correlated with the ratio of NO₂⁻/NO₃⁻ concentrations (Figure S8). Intracellularly produced NO₂⁻ does not seem to exchange with the surrounding pool, but ambient NO₃⁻ is directly converted to N₂O, a process identified as “NO₂⁻ shunting” in N₂ production studies (de Brabandere et al. 2014, Chang et al. 2014). POM as electron donor is an important regulator for reductive N₂O production.

4.4 Effect of abundance of total and active community composition on N₂O production rates

655 The abundances of both *amoA* and *nirS* genes found in the ETSP are similar to those reported in earlier studies in the ETSP (Peng et al. 2013, Ji et al. 2015a, Jayakumar et al. 2013). The *amoA* gene abundances were similar to those reported for the coastal ETSP by Lam et al. (2009), but *nirS* abundances reported here were higher than the *nirS* abundances in that study, probably due to the use of different PCR primers. The community composition of AOA did not significantly differ along the O₂ gradient as shown previously (Peng et al. 2013), but a significant correlation between archaeal *amoA* transcript abundance and N₂O production was shown in this study. 660 The combination of qPCR and microarray analysis offered a great advantage to relate the total abundances to the production rates and additionally link particular community components to biogeochemical activities. To determine whether a particular archetype drives the correlation of N₂O production by AO, a Bray-Curtis dissimilarity matrix revealed archetype AOA3 related to *Nitrosopelagicus brevis* (CN25) to be significantly correlated with the N₂O production by AO. This clade is abundant in the surface ocean and typically found in high 665 abundances in the lower euphotic zone (Santoro et al. 2011, 2015). With the demonstration of high abundances of AOA3 coincident with high nitrification rates and high N₂O production rates, we suggest that *Nitrosopelagicus brevis* related AOA likely play an important role in N₂O production in near surface waters in the Eastern Tropical South Pacific.

670 The lack of significant correlation between community composition or single members of the community and reductive N₂O production is consistent with the fact that *nirS* is not the enzyme directly synthesizing N₂O and *nirS* communities are sources as well as sinks for N₂O. Taxonomic analysis of the *nirS* gene and transcripts suggested that there is high taxonomic diversity among the denitrifiers, which is likely linked to a high variability 675 of the total denitrification gene assembly (including *nos*, *nor*, *nir*). In particular the abundance and diversity of nitric oxide reductase (*nor*), the enzyme directly synthesizing N₂O, would be of interest, but it is present in nitrifiers and denitrifiers (Casciotti and Ward 2005) and one goal of this study was to differentiate among N₂O produced by nitrifiers and denitrifiers. However, *nirS* gene and transcript abundance correlated with N₂O production from NO₂⁻ making it a possible indicator for one part of reductive N₂O production. It is also worth noting that anammox related *nirS* genes and transcripts (*nirS* 166, 167) contribute up to 12% of the total copy numbers putting a wrinkle 680 on *nirS* abundance as marker gene for denitrifiers only. The subtraction of the anammox related *nirS* genes from total copy numbers did not change the results from Bray-Curtis Analysis. These data indicate that the extent to

which gene or transcript abundance patterns or community composition of marker genes of processes can be used as proxies for process rate measurements is variable, likely due to complex factors, including the relative dominance of different community members, the modular nature of denitrification, differences in the level of metabolic regulation (transcriptional, translational, and enzymatic), and the range of environmental conditions being observed.

4.5 Summary and conclusion

In this study we used a combined approach of ^{15}N tracer techniques and molecular techniques in order to investigate the factors that control N_2O production within the upper oxycline of the ODZ in the ETSP. Our results suggest that denitrification is a major N_2O source along the oxic - anoxic interface of the upper oxycline. Highest N_2O production rates from NO_2^- and NO_3^- were found at or below the oxic-anoxic interface, whereas highest N_2O production from AO was slightly shallower in the oxycline. Overall, *in situ* O_2 threshold below 8 $\mu\text{mol L}^{-1}$ favored NO_3^- and NO_2^- reduction to N_2O and high N_2O yields from AO up to 2.2%. A different pattern was observed for the community response to increasing oxygen, with highest N_2O production from NH_4^+ and NO_2^- between 1.4 – 6 $\mu\text{mol L}^{-1}$ O_2 and high N_2O production from NO_3^- even at O_2 concentrations up to 22 $\mu\text{mol L}^{-1}$. This study highlights the diversity of N_2O production regulation and the need to conduct further experiments where single community members can be better constrained. Our experiments provide the first insights into N_2O regulation by particulate organic matter in the ETSP with particles greatly enhancing N_2O production (up to 5fold). Furthermore, the significant positive correlation between *Nitrosopelagicus brevis* (CN25) and N_2O produced from AO could indicate its importance in N_2O production and points out the great value of combining biogeochemical rate measurements with molecular analysis to investigate multifaceted N_2O cycling. This study shows that short term oxygen increase can lead to high N_2O production even from denitrification and extends the existing O_2 thresholds for high reductive N_2O production up to 22 $\mu\text{mol L}^{-1}$ O_2 . Together with high N_2O yields from AO up to O_2 levels of 30 $\mu\text{mol L}^{-1}$, an expansion of low oxygenated waters around ODZs predicted for the future can significantly increase marine N_2O production.

Regardless of which processes are responsible for N_2O production in the ODZ, high N_2O production at the oxic-anoxic interface of the upper oxycline sustains high N_2O concentration peaks with a potential for intense N_2O emission to the atmosphere during upwelling events. An average total N_2O production rate of 3.1 $\text{nmol N}_2\text{O L}^{-1} \text{ d}^{-1}$ in a 50 m thick suboxic layer with 0 – 20 $\mu\text{mol L}^{-1}$ O_2 leads to an annual N_2O efflux of 0.5 Tg N y^{-1} in the Peruvian upwelling ($2.22 \times 10^5 \text{ km}^2$, Arévalo-Martínez et al. 2015), which is within the estimates based on surface N_2O concentration measurements from 2012-2013 (Arévalo-Martínez et al. 2015, Bourbonnais et al. 2017). The importance of the Peru upwelling system for global N_2O emissions (5 – 22% of global marine N_2O emissions) is directly linked to the extreme N_2O accumulations in coastal waters. Coastal N_2O hotspots are well known (Bakker et al. 2014) and this study shows that they can be explained by considering denitrification as a major N_2O source. While this study does not help to resolve temporal variability, manipulation experiments give valuable insights into the short-term response of N_2O production to oxygen and particles. With the further parametrization of POM export as a driver for N_2O production from denitrification, models may be able to better predict N_2O emissions in highly productive coastal upwelling regions and to evaluate how fluxes might change with changing stratification and deoxygenation.

Data availability: The data presented here were archived in the SFB754 database (www.sfb754.de). The N₂O data are also available from the Marine Methane and Nitrous Oxide (MEMENTO) database (<https://memento.geomar.de/de/n2o>).

725 **Author contributions:** CF, HWB and BW conceptualized the study. CF and MS performed experiment. CF and ELP analyzed samples. RX and EA collected POM. DLAM sampled and measured N₂O concentrations. AJ performed qPCR. SO supported mass spectrometer analysis. XS supported experimental methods and assisted with data analysis. CF analyzed data and led the writing effort, with substantial contributions from all co-authors.

Competing interests: Authors declare no competing interests.

730 **Acknowledgement:** The work presented here was made possible by the DFG-funded Joint Collaborative Centre SFB754 Phase III (<http://www.sfb754.de>) and by a fellowship of the German Academic Exchange Service (DAAD) program 'Postdoctoral Researchers International Mobility Experience (PRIME, ID 57350888) awarded to CF. MS was supported by the China Scholarship Council (No. 201406330054). E.L-P had a FPU-PhD fellowship (014/02917) from the Spanish Ministry of Education and a PhD International Mobility scholarship 735 from the Universidad de Granada. CRL was funded by a EU H2020 Marie Curie Individual Fellowship (NITROX, Grant #704272) and by the Villum Foundation (Grant# 16518). EA, HWB and RX were funded by the DFG-funded Joint Collaborative Centre SFB754 program. We thank the captain and crew of R/V Meteor. Moreover, we thank the Peruvian authorities for the permission to work in their territorial waters.

740

References

745 Anderson, J. H. (1964). The metabolism of hydroxylamine to nitrite by *Nitrosomonas*. *Biochemistry Journal*, 91(1948), 8–17. <https://doi.org/10.1042/bj0910008>

750 Arévalo-Martínez, D. L., Kock, A., Löscher, C. R., Schmitz, R. A., Bange, H. W., Arevalo-Martínez, D., ... Bange, H. W. (2015). Massive nitrous oxide emissions from the tropical South Pacific Ocean. *Nature Geoscience*, 8(7), 530–533. <https://doi.org/10.1038/NGEO2469>

755 Arévalo-Martínez, Damian L., Kock, A., Löscher, C. R., Schmitz, R. A., Stramma, L., & Bange, H. W. (2016). Influence of mesoscale eddies on the distribution of nitrous oxide in the eastern tropical South Pacific. *Biogeosciences*, 13(4), 1105–1118. <https://doi.org/10.5194/bg-13-1105-2016>

760 Babbin, A. R., Bianchi, D., Jayakumar, A., & Ward, B. B. (2015). Rapid nitrous oxide cycling in the suboxic ocean. *Science*, 348(6239), 1127–1129. <https://doi.org/10.1126/science.aaa8380>

765 Babbin, A. R., Keil, R. G., Devol, A. H., & Ward, B. B. (2014). Organic matter stoichiometry, flux, and oxygen control nitrogen loss in the ocean. *Science (New York, N.Y.)*, 344(6182), 406–408. <https://doi.org/10.1126/science.1248364>

770 Bakker, D. C. E., Bange, H. W., Gruber, N., Johannessen, T., Upstill-Goddard, R. C., Borges, A. V., ... Santana-Casiano, J. M. (2014). Air-Sea Interactions of Natural Long-Lived Greenhouse Gases (CO_2 , N_2O , CH_4) in a Changing Climate. In *Ocean-Atmosphere Interactions of Gases and Particles* (pp. 55–112). <https://doi.org/10.1007/978-3-642-25643-1>

775 Bange, H. W. (2008). Gaseous nitrogen compounds (NO , N_2O , N_2 , NH_3) in the ocean. In *Nitrogen in the marine environment* (pp. 51–94). Amsterdam: Elsevier.

780 Battaglia, G., & Joos, F. (2018). Marine N_2O Emissions From Nitrification and Denitrification Constrained by Modern Observations and Projected in Multimillennial Global Warming Simulations. *Global Biogeochemical Cycles*, 32(1), 92–121. <https://doi.org/10.1002/2017GB005671>

785 Beman, J. M., Chow, C., King, A. L., Feng, Y., & Fuhrman, J. a. (2011). Global declines in oceanic nitrification rates as a consequence of ocean acidification. *Proceedings of the National Academy of Sciences of the United States of America*, 108(1), 208–213. <https://doi.org/10.1073/pnas.1011053108/-/DCSupplemental.www.pnas.org/cgi/doi/10.1073/pnas.1011053108>

790 Bertagnolli, A. D., & Ulloa, O. (2017). Hydrography shapes community composition and diversity of amoA-containing Thaumarchaeota in the coastal waters off central Chile. *Environmental Microbiology Reports*, 9(6), 717–728. <https://doi.org/10.1111/1758-2229.12579>

795 Biller, S. J., Mosier, A. C., Wells, G. F., & Francis, C. A. (2012). Global Biodiversity of Aquatic Ammonia-Oxidizing Archaea is Partitioned by Habitat. *Frontiers in Microbiology*, 3, 252. <https://doi.org/10.3389/fmicb.2012.00252>

800 Blum, J. M., Su, Q., Ma, Y., Valverde-Pérez, B., Domingo-Félez, C., Jensen, M. M., & Smets, B. F. (2018). The pH dependency of N-converting enzymatic processes, pathways and microbes: effect on net N_2O production. *Environmental Microbiology*, 20(5), 1623–1640. <https://doi.org/10.1111/1462-2920.14063>

Bonaglia, S., Klawonn, I., De Brabandere, L., Deutsch, B., Thamdrup, B., & Brüchert, V. (2016). Denitrification and DNRA at the Baltic Sea oxic–anoxic interface: Substrate spectrum and kinetics. *Limnology and Oceanography*, 61(5), 1900–1915. <https://doi.org/10.1002/limo.10343>

Borcard, D., Legendre, P., & Drapeau, P. (1992). Partialling out the Spatial Component of Ecological Variation. *Ecology*, 73(3), 1045–1055. <https://doi.org/10.2307/1940179>

Bourbonnais, A., Altabet, M. A., Charoenpong, C. N., Larkum, J., Hu, H., Bange, H. W., & Stramma, L. (2015). N-loss isotope effects in the Peru oxygen minimum zone studied using a mesoscale eddy as a natural tracer experiment. *Global Biogeochemical Cycles*, 29, 793–811. <https://doi.org/10.1002/2014GB005001>

Bourbonnais, A., Letscher, R. T., Bange, H. W., Échevin, V., Larkum, J., Mohn, J., ... Altabet, M. A. (2017). N_2O production and consumption from stable isotopic and concentration data in the Peruvian coastal upwelling system. *Global Biogeochemical Cycles*, 31(4), 678–698. <https://doi.org/10.1002/2016GB005567>

Bouskill, N. J., Eveillard, D., O'Mullan, G., Jackson, G. A., & Ward, B. B. (2011). Seasonal and annual reoccurrence in betaproteobacterial ammonia-oxidizing bacterial population structure. *Environmental Microbiology*, 13(4), 872–886. <https://doi.org/10.1111/j.1462-2920.2010.02362.x>

Boyd, P. W., Sherry, N. D., Berge, J. A., Bishop, J. K. B., Calvert, S. E., Charette, M. A., ... Wong, C. S. (1999). Transformations of biogenic particulates from the pelagic to the deep ocean realm. *Deep Sea Research Part II: Topical Studies in Oceanography*, 46(11–12), 2761–2792. [https://doi.org/10.1016/S0967-0645\(99\)00083-1](https://doi.org/10.1016/S0967-0645(99)00083-1)

Braker, G., Fesefeldt, A., & Witzel, K. P. (1998). Development of PCR primer systems for amplification of nitrite reductase genes (*nirK* and *nirS*) to detect denitrifying bacteria in environmental samples. *Applied and Environmental Microbiology*, 64(10), 3769–3775.

Breider, F., Yoshikawa, C., Makabe, A., Toyoda, S., Wakita, M., Matsui, Y., ... Yoshida, N. (2019). Response of N_2O production rate to ocean acidification in the western North Pacific. *Nature Climate Change*, 9(12), 954–958. <https://doi.org/10.1038/s41558-019-0605-7>

Bristow, L A, Callbeck, C. M., Larsen, M., Altabet, M. A., Dekaezemacker, J., Forth, M., ... Canfield, D. E.

805 (2016a). N₂ production rates limited by nitrite availability in the Bay of Bengal oxygen minimum zone. *Nature Geosci., advance on*(December). <https://doi.org/10.1038/ngeo2847>

Bristow, Laura A., Dalsgaard, T., Tiano, L., Mills, D. B., Bertagnolli, A. D., Wright, J. J., ... Thamdrup, B. (2016b). Ammonium and nitrite oxidation at nanomolar oxygen concentrations in oxygen minimum zone waters. *Proceedings of the National Academy of Sciences*, 113(38), 201600359.

810 Buitenhuis, E. T., Suntharalingam, P., & Le Quéré, C. (2018). Constraints on global oceanic emissions of N₂O from observations and models. *Biogeosciences*, 15(7), 2161–2175. <https://doi.org/10.5194/bg-15-2161-2018>

Callbeck, C. M., Lavik, G., Ferdelman, T. G., Fuchs, B., Gruber-Vodicka, H. R., Hach, P. F., ... Kuypers, M. M. M. (2018). Oxygen minimum zone cryptic sulfur cycling sustained by offshore transport of key sulfur oxidizing bacteria. *Nature Communications*, 9(1), 1–11. <https://doi.org/10.1038/s41467-018-04041-x>

815 Capone, D. G., & Hutchins, D. A. (2013). Microbial biogeochemistry of coastal upwelling regimes in a changing ocean. *Nature Geoscience*, 6(9), 711–717. <https://doi.org/10.1038/ngeo1916>

Caranto, J. D., Lancaster, K. M., Ma, C., Jensen, M. M., Smets, B. F., Thamdrup, B., ... Lancaster, K. M. (2017). Nitric oxide is an obligate bacterial nitrification intermediate produced by hydroxylamine oxidoreductase. *Proceedings of the National Academy of Sciences*, 114(31), 8217–8222. <https://doi.org/10.1073/pnas.1704504114>

820 Carini, P., Dupont, C. L., & Santoro, A. E. (2018). Patterns of thaumarchaeal gene expression in culture and diverse marine environments. *Environmental Microbiology*. <https://doi.org/10.1111/1462-2920.14107>

Carrasco, C., Karstensen, J., & Farias, L. (2017). On the Nitrous Oxide Accumulation in Intermediate Waters of the Eastern South Pacific Ocean. *Frontiers in Marine Science*, 4, 24. <https://doi.org/10.3389/fmars.2017.00024>

825 Casciotti, L., & Ward, B. (2005). Phylogenetic analysis of nitric oxide reductase gene homologues from aerobic ammonia-oxidizing bacteria. *FEMS Microbiology Ecology*, 52(2), 197–205. <http://dx.doi.org/10.1016/j.femsec.2004.11.002>

Casciotti, K. L., Forbes, M., Vedamati, J., Peters, B., Martin, T., & Mordy, C. W. (2018). Nitrous oxide cycling in the Eastern Tropical South Pacific as inferred from isotopic and isotopomeric data. *Deep Sea Research Part II: Topical Studies in Oceanography*, (xxxx), 1–13. <https://doi.org/10.1016/J.DSR2.2018.07.014>

830 Chang, B. X., Rich, J. R., Jayakumar, A., Naik, H., Pratihary, A., Keil, R. G., ... Devol, A. H. (2014). The effect of organic carbon on fixed nitrogen loss in the eastern tropical South Pacific and Arabian Sea oxygen deficient zones. *Limnology and Oceanography*, 59(4), 1267–1274. <https://doi.org/10.4319/lo.2014.59.4.1267>

Charpentier, J., Farias, L., Yoshida, N., Boontanon, N., & Raimbault, P. (2007). Nitrous oxide distribution and its origin in the central and eastern South Pacific Subtropical Gyre. *Biogeosciences*, 4(5), 729–741. <https://doi.org/10.5194/bg-4-729-2007>

835 Chavez, F. P., & Messié, M. (2009). A comparison of Eastern Boundary Upwelling Ecosystems. *Progress in Oceanography*, 83(1–4), 80–96. <https://doi.org/10.1016/j.pocean.2009.07.032>

Codispoti, L. A. (2010). Interesting Times for Marine N₂O. *Science*, 332, 1339–1340.

Cohen, Y., & Gordon, L. (1978). Nitrous oxide in the oxygen minimum of eastern tropical North Pacific: evidence for its consumption during denitrification and possible mechanisms for its production. *Deep Sea Research*, 25(1977), 509–524.

840 Cornejo DOttone, M., Bravo, L., Ramos, M., Pizarro, O., Karstensen, J., Gallegos, M., ... Karp-Boss, L. (2016). Biogeochemical characteristics of a long-lived anticyclonic eddy in the eastern South Pacific Ocean. *Biogeosciences*, 13(10), 2971–2979. <https://doi.org/10.5194/bg-13-2971-2016>

Crutzen, P. J. (1970). The influence of nitrogen oxides on the atmospheric ozone content. *Quarterly Journal of the Royal Meteorological Society*, 96(408), 320–325. <https://doi.org/10.1002/qj.49709640815>

845 Dalsgaard, T., Stewart, F. J., Thamdrup, B., De Brabandere, L., Revsbech, N. P., Ulloa, O., ... Delong, E. F. (2014). Oxygen at nanomolar levels reversibly suppresses process rates and gene expression in anammox and denitrification in the oxygen minimum zone off northern Chile. *MBio*, 5(6), e01966. <https://doi.org/10.1128/mBio.01966-14>

Dalsgaard, T., Thamdrup, B., Farías, L., Peter Revsbech, N., & Revsbech, N. P. (2012). Anammox and denitrification in the oxygen minimum zone of the eastern South Pacific. *Limnology and Oceanography*, 57(5), 1331–1346. <https://doi.org/10.4319/lo.2012.57.5.1331>

850 De Brabandere, L., Canfield, D. E., Dalsgaard, T., Friederich, G. E., Revsbech, N. P., Ulloa, O., & Thamdrup, B. (2014). Vertical partitioning of nitrogen-loss processes across the oxic-anoxic interface of an oceanic oxygen minimum zone. *Environmental Microbiology*, 16(10), 3041–3054. <https://doi.org/10.1111/1462-2920.12255>

Farías, L., Castro-González, M., Cornejo, M., Charpentier, J. J., Faúndez, J., Boontanon, N., ... Yoshida, N. (2009). Denitrification and nitrous oxide cycling within the upper oxycline of the eastern tropical South Pacific oxygen minimum zone. *Limnology and Oceanography*, 54(1), 132–144. <https://doi.org/10.4319/lo.2009.54.1.0132>

860 865 Frame, C. H., & Casciotti, K. L. (2010). Biogeochemical controls and isotopic signatures of nitrous oxide

production by a marine ammonia-oxidizing bacterium. *Biogeosciences*, 7, 3019–3059. <https://doi.org/10.5194/bg-7-2695-2010>

Frame, C. H., Lau, E., Nolan, E. J., Goepfert, T. J., & Lehmann, M. F. (2017). Acidification Enhances Hybrid N₂O Production Associated with Aquatic Ammonia-Oxidizing Microorganisms. *Frontiers in Microbiology*, 7(January), 2104. <https://doi.org/10.3389/fmicb.2016.02104>

Francis, C. A., Roberts, K. J., Beman, J. M., Santoro, A. E., & Oakley, B. B. (2005). Ubiquity and diversity of ammonia-oxidizing archaea in water columns and sediments of the ocean. *Proceedings of the National Academy of Sciences*, 102(41), 14683–14688. <https://doi.org/10.1073/pnas.0506625102>

Ganesh, S., Parris, D. J., Delong, E. F., & Stewart, F. J. (2014). Metagenomic analysis of size-fractionated picoplankton in a marine oxygen minimum zone. *ISME Journal*, 8(1), 187–211. <https://doi.org/10.1038/ismej.2013.144>

Goreau, T. J., Kaplan, W. A., Wofsy, S. C., McElroy, M. B., Valois, F. W., & Watson, S. W. (1980). Production of NO₂⁻ and N₂O by Nitrifying Bacteria at Reduced Concentrations of Oxygen. *Appl. Environ. Microbiol.*, 40(3), 526–532.

Goréguès, C., Michotey, V., & Bonin, P. (2004). Isolation of hydrocarbonoclastic denitrifying bacteria from berre microbial mats. *Ophelia*, 58(3), 263–270. <https://doi.org/10.1080/00785236.2004.10410234>

Granger, J., & Ward, B. B. (2003). Accumulation of nitrogen oxides in copper-limited cultures of denitrifying bacteria. *Limnology and Oceanography*, 48(1), 313–318. <https://doi.org/10.4319/lo.2003.48.1.0313>

Hamdan, L. J., Coffin, R. B., Sikaroodi, M., Greinert, J., Treude, T., & Gillevet, P. M. (2012). Ocean currents shape the microbiome of Arctic marine sediments. *The ISME Journal*, 7(4), 685–696. <https://doi.org/10.1038/ismej.2012.143>

Hammer, Ø., HARPER, D. A. T., & Ryan, P. D. (2001). PAST: Paleontological statistics software package. *Palaeontologia Electronica*, 4(1), 1–9. <https://doi.org/10.1016/j.bcp.2008.05.025>

Haskell, W. Z., Kadko, D., Hammond, D. E., Knapp, A. N., Prokopenko, M. G., Berelson, W. M., & Capone, D. G. (2015). Upwelling velocity and eddy diffusivity from ⁷Be measurements used to compare vertical nutrient flux to export POC flux in the Eastern Tropical South Pacific. *Marine Chemistry*, 168, 140–150. <https://doi.org/10.1016/J.MARCHEM.2014.10.004>

Hink, L., Lycus, P., Gubry-Rangin, C., Frostegård, Å., Nicol, G. W., Prosser, J. I., & Bakken, L. R. (2017)a. Kinetics of NH₃-oxidation, NO-turnover, N₂O-production and electron flow during oxygen depletion in model bacterial and archaeal ammonia oxidisers. *Environmental Microbiology*, 19(12), 4882–4896. <https://doi.org/10.1111/1462-2920.13914>

Hink, L., Nicol, G. W., & Prosser, J. I. (2017)b. Archaea produce lower yields of N₂O than bacteria during aerobic ammonia oxidation in soil. *Environmental Microbiology*, 19(12), 4829–4837. <https://doi.org/10.1111/1462-2920.13282>

Holmes, R. M., Aminot, A., Kéruel, R., Hooker, B. A., & Peterson, B. J. (1999). A simple and precise method for measuring ammonium in marine and freshwater ecosystems. *Canadian Journal of Fisheries and Aquatic Sciences*, 56, 1802–1808.

Hu, H., Bourbonnais, A., Larkum, J., Bange, H. W., & Altabet, M. A. (2016). Nitrogen cycling in shallow low-oxygen coastal waters off Peru from nitrite and nitrate nitrogen and oxygen isotopes. *Biogeosciences*, 13(5), 1453–1468. <https://doi.org/10.5194/bg-13-1453-2016>

Hu, Z., Wessels, H. J. C. T., Alen, T., Jetten, M. S. M., & Kartal, B. (2019). Nitric oxide-dependent anaerobic ammonium oxidation. *Nature Communications*, 10(1244), 1–7. <https://doi.org/10.1038/s41467-019-09268-w>

Hydes, D., Aoyama, M., Aminot, A., Bakker, K., Becker, S., Coverly, S., ... Zhang, J. Z. (2010). Determination of dissolved nutrients (N, P, Si) in seawater with high precision and inter-comparability using gas-segmented continuous flow analysers. *The GO-SHIP Repeat Hydrography Manual IOCCP Report*, 134(14), 1–87.

IPCC. (2013). *Climate Change 2013: The Physical Science Basis. Contribution of Working Group I to the Fifth Assessment Report of the Intergovernmental Panel on Climate Change*. Cambridge UK and New York, USA: Cambridge University Press. <https://doi.org/10.1017/CBO9781107415324.010>

Jayakumar, A., Peng, X., & Ward, B. (2013). Community composition of bacteria involved in fixed nitrogen loss in the water column of two major oxygen minimum zones in the ocean. *Aquatic Microbial Ecology*, 70(3), 245–259. <https://doi.org/10.3354/ame01654>

Jayakumar, D. A., Naqvi, S. W. A., & Ward, B. B. (2009). Distribution and relative quantification of key genes involved in fixed nitrogen loss from the Arabian Sea oxygen minimum zone. *Indian Ocean Biogeochemical Processes and Ecological Variability*, 187–203.

Jebaraj, C. S., Forster, D., Kauff, F., & Stoeck, T. (2012). Molecular Diversity of Fungi from Marine Oxygen-Deficient Environments (ODEs) (pp. 189–208). Springer, Berlin, Heidelberg. https://doi.org/10.1007/978-3-642-23342-5_10

Jetten, M. S. M., Ward, B. B., & Jensen, M. M. (2008). The microbial nitrogen cycle. *Environmental Microbiology*, 10(11), 2903–2909. <https://doi.org/10.1111/j.1462-2920.2008.01786.x>

Ji, Q., Babbin, A. R., Jayakumar, A., & Ward, B. B. (2015a). Nitrous oxide production by nitrification and

denitrification in the Eastern Tropical South Pacific oxygen minimum zone. *Geophysical Research Letters*. <https://doi.org/10.1002/2015GL066853>

930 Ji, Q., Babbin, A. R., Peng, X., Bowen, J. L., Ward, B. B., & Ji, Q. (2015b). Nitrogen substrate-dependent nitrous oxide cycling in salt marsh sediments. *Journal of Marine Research*, 73(73), 71–92.

Ji, Q., Buitenhuis, E., Suntharalingam, P., Sarmiento, J. L., & Ward, B. B. (2018). Global nitrous oxide production determined by oxygen sensitivity of nitrification and denitrification. <https://doi.org/10.1029/2018GB005887>

935 Ji, Q., Frey, C., Sun, X., Jackson, M., Lee, Y., Jayakumar, A., ... Ward, B. B. (2018). Nitrogen and oxygen availabilities control water column nitrous oxide production during seasonal anoxia in the Chesapeake Bay, (March), 6127–6138.

Johnston, H. (1971). Reduction of Stratospheric Ozone by Nitrogen Oxide Catalysts from Supersonic Transport Exhaust. *Science (New York, N.Y.)*, 173, 517–522.

940 Jr., D. J. M., Anderson, L. A., Bates, N. R., Bibby, T., Buesseler, K. O., Carlson, C. A., ... Steinberg, D. K. (2007). Eddy / Wind Interactions Stimulate Extraordinary Mid-Ocean Plankton Blooms. *Science*, 316, 1021–1026. <https://doi.org/10.1126/science.1136256>

Kalvelage, T., Jensen, M. M., Contreras, S., Revsbech, N. P., Lam, P., Günter, M., ... Kuypers, M. M. M. M. (2011). Oxygen sensitivity of anammox and coupled N-cycle processes in oxygen minimum zones. *PLoS ONE*, 6(12), e29299. <https://doi.org/10.1371/journal.pone.0029299>

945 Kalvelage, T., Lavik, G., Jensen, M. M., Revsbech, N. P., Loescher, C., Schunck, H., ... Kuypers, M. M. M. M. (2015). Aerobic Microbial Respiration In Oceanic Oxygen Minimum Zones. *Plos One*, 10(7). <https://doi.org/e013352610.1371/journal.pone.0133526>

950 Kartal, B., Kuypers, M. M. M., Lavik, G., Schalk, J., Op den Camp, H. J. M., Jetten, M. S. M., & Strous, M. (2007). Anammox bacteria disguised as denitrifiers: nitrate reduction to dinitrogen gas via nitrite and ammonium. *Environmental Microbiology*, 9(3), 635–642. <https://doi.org/10.1111/j.1462-2920.2006.01183.x>

Klawonn, I., Bonaglia, S., Whitehouse, M. J., Littmann, S., Tienken, D., Kuypers, M. M. M., ... Ploug, H. (2019). Untangling hidden nutrient dynamics: rapid ammonium cycling and single-cell ammonium assimilation in marine plankton communities. *The ISME Journal*. <https://doi.org/10.1038/s41396-019-0386-z>

955 Kock, A., Arévalo-Martínez, D. L., Löscher, C. R., & Bange, H. W. (2016). Extreme N₂O accumulation in the coastal oxygen minimum zone off Peru. *Biogeosciences*, 13(3), 827–840. <https://doi.org/10.5194/bg-13-827-2016>

960 Kondo, Y., & Moffett, J. W. (2015). Iron redox cycling and subsurface offshore transport in the eastern tropical South Pacific oxygen minimum zone. *Marine Chemistry*, 168, 95–103. <https://doi.org/10.1016/J.MARCHEM.2014.11.007>

Körner, H., & Zumft, W. G. (1989). Expression of denitrification enzymes in response to the dissolved oxygen level and respiratory substrate in continuous culture of *Pseudomonas stutzeri*. *Applied and Environmental Microbiology*, 55(7), 1670–1676.

965 Korth, F., Kock, A., Arévalo-Martínez, D. L., & Bange, H. W. (2019). Hydroxylamine as a Potential Indicator of Nitrification in the Open Ocean. *Geophysical Research Letters*, 46(4), 2158–2166. <https://doi.org/10.1029/2018GL080466>

Kozlowski, J. A., Stieglmeier, M., Schleper, C., Klotz, M. G., & Stein, L. Y. (2016). Pathways and key intermediates required for obligate aerobic ammonia-dependent chemolithotrophy in bacteria and Thaumarchaeota. *The ISME Journal*, 10(8), 1–10. <https://doi.org/10.1038/ismej.2016.2>

970 Lam, Lavik, G., Jensen, M. M., Vossenberg, J. van de, Schmid, M., Woebken, D., ... Kuypers, M. M. M. (2009). Revising the nitrogen cycle in the Peruvian oxygen minimum zone. *Proceedings of the National Academy of Sciences*, 106(12), 4752–4757.

975 Lancaster, K. M., Caranto, J. D., Majer, S. H., & Smith, M. A. (2018). Alternative Bioenergy : Updates to and Challenges in Nitrification Metalloenzymology. *Joule*, 2(3), 421–441. <https://doi.org/10.1016/j.joule.2018.01.018>

Landolfi, A., Somes, C. J., Koeve, W., Zamora, L. M., & Oschlies, A. (2017). Oceanic nitrogen cycling and N₂O flux perturbations in the Anthropocene. *Global Biogeochemical Cycles*, 31(8), 1236–1255. <https://doi.org/10.1002/2017GB005633>

980 Larsen, M., Lehner, P., Borisov, S. M., Klimant, I., Fischer, J. P., Stewart, F. J., ... Glud, R. N. (2016). In situ quantification of ultra-low O₂ concentrations in oxygen minimum zones: Application of novel optodes. *Limnology and Oceanography: Methods*, 14(12), 784–800. <https://doi.org/10.1002/lom3.10126>

Legendre, P., & Legendre, L. (2012). *Numerical ecology*. New York, NY, USA: Elsevier.

985 Liu, Z., Stewart, G., Kirk Cochran, J., Lee, C., Armstrong, R. A., Hirschberg, D. J., ... Miquel, J.-C. (2005). Why do POC concentrations measured using Niskin bottle collections sometimes differ from those using in-situ pumps? *Deep Sea Research Part I: Oceanographic Research Papers*, 52(7), 1324–1344. <https://doi.org/10.1016/J.DSR.2005.02.005>

Löscher, C. R., Kock, A., Könneke, M., LaRoche, J., Bange, H. W., & Schmitz, R. A. (2012). Production of

990 oceanic nitrous oxide by ammonia-oxidizing archaea. *Biogeosciences*, 9(7), 2419–2429. <https://doi.org/10.5194/bg-9-2419-2012>

995 Löscher, Carolin R., Bange, H. W., Schmitz, R. A., Callbeck, C. M., Engel, A., Hauss, H., ... Wagner, H. (2016). Water column biogeochemistry of oxygen minimum zones in the eastern tropical North Atlantic and eastern tropical South Pacific oceans. *Biogeosciences*, 13(12), 3585–3606. <https://doi.org/10.5194/bg-13-3585-2016>

1000 Lutterbeck, H. E., Arévalo-Martínez, D. L., Löscher, C. R., & Bange, H. W. (2018). Nitric oxide (NO) in the oxygen minimum zone off Peru. *Deep Sea Research Part II: Topical Studies in Oceanography*, (xxxx), 0–1. <https://doi.org/10.1016/j.dsr2.2017.12.023>

1005 Martin, J. H., Knauer, G. A., Karl, D. M., & Broenkow, W. W. (1987). VERTEX: carbon cycling in the northeast Pacific. *Deep Sea Research Part A. Oceanographic Research Papers*, 34(2), 267–285. [https://doi.org/10.1016/0198-0149\(87\)90086-0](https://doi.org/10.1016/0198-0149(87)90086-0)

1010 Martinez-Rey, J., Bopp, L., Gehlen, M., Tagliabue, A., & Gruber, N. (2015). Projections of oceanic N_2O emissions in the 21st century using the IPSL Earth system model. *Biogeosciences*, 12(13), 4133–4148. <https://doi.org/10.5194/bg-12-4133-2015>

1015 McIlvin, M. R., & Altabet, M. A. (2005). Chemical Conversion of Nitrate and Nitrite to Nitrous Oxide for Nitrogen and Oxygen Isotopic Analysis in Freshwater and Seawater. *Analytical Chemistry*, 77(17), 5589–5595.

1020 McKenney, D. J., Drury, C. F., Findlay, W. I., Mutus, B., McDonnell, T., & Gajda, C. (1994). Kinetics of denitrification by *Pseudomonas fluorescens*: Oxygen effects. *Soil Biology and Biochemistry*, 26(7), 901–908.

1025 Messié, M., & Chavez, F. P. (2015). Seasonal regulation of primary production in eastern boundary upwelling systems. *Progress in Oceanography*, 134, 1–18. <https://doi.org/10.1016/j.pocean.2014.10.011>

1030 Mincer, T. J., Church, M. J., Taylor, L. T., Preston, C., Karl, D. M., & DeLong, E. F. (2007). Quantitative distribution of presumptive archaeal and bacterial nitrifiers in Monterey Bay and the North Pacific Subtropical Gyre. *Environmental Microbiology*, 9(5), 1162–1175. <https://doi.org/10.1111/j.1462-2920.2007.01239.x>

1035 Murdock, S. A., & Juniper, S. K. (2017). Capturing Compositional Variation in Denitrifying Communities: a Multiple- Primer Approach That Includes Epsilonproteobacteria. *Applied and Environmental Microbiology*, 83(6), 1–16.

1040 Newell, S. E., Babbin, A. R., Jayakumar, A., & Ward, B. B. (2011). Ammonia oxidation rates and nitrification in the Arabian Sea. *Global Biogeochemical Cycles*, 25(4), 1–10. <https://doi.org/10.1029/2010gb003940>

1045 Nicholls, J. C., Davies, C. A., & Trimmer, M. (2007). High-resolution profiles and nitrogen isotope tracing reveal a dominant source of nitrous oxide and multiple pathways of nitrogen gas formation in the central Arabian Sea. *Limnology and Oceanography*, 52(1), 156–168. <https://doi.org/10.4319/lo.2007.52.1.0156>

1050 Oksanen, J., Blanchet, F. G., Friendly, M., Kindt, R., Legendre, P., Mcglinn, D., ... Maintainer, H. W. (2019). Package “vegan” Title Community Ecology Package. *Community Ecology Package*, 2(9), 1–297.

1055 Peng, X., Jayakumar, A., & Ward, B. B. (2013). Community composition of ammonia-oxidizing archaea from surface and anoxic depths of oceanic oxygen minimum zones. *Frontiers in Microbiology*, 4(JUL), 1–12. <https://doi.org/10.3389/fmicb.2013.00177>

1060 Pietri, A., Testor, P., Echevin, V., Chaigneau, A., Mortier, L., Eldin, G., ... Grados, C. (2013). Finescale Vertical Structure of the Upwelling System off Southern Peru as Observed from Glider Data. *Journal of Physical Oceanography*, 43(3), 631–646. <https://doi.org/10.1175/JPO-D-12-035.1>

1065 Qin, W., Meinhardt, K. A., Moffett, J. W., Devol, A. H., Armbrust, E. V., Ingalls, A. E., & Stahl, D. A. (2017). Influence of Oxygen Availability on the Activities of Ammonia-oxidizing Archaea. *Environmental Microbiology Reports*. <https://doi.org/10.1111/1758-2229.12525>

1070 Ravishankara, A. R., Daniel, J. S., & Portmann, R. W. (2009). Nitrous oxide (N_2O): the dominant ozone-depleting substance emitted in the 21st century. *Science (New York, N.Y.)*, 326(5949), 123–125. <https://doi.org/10.1126/science.1176985>

1075 Richards, T. A., Jones, M. D. M., Leonard, G., & Bass, D. (2012). Marine Fungi: Their Ecology and Molecular Diversity. *Annual Review of Marine Science*, 4(1), 495–522. <https://doi.org/10.1146/annurev-marine-120710-100802>

1080 Ryabenco, E., Kock, a., Bange, H. W., Altabet, M. a., & Wallace, D. W. R. (2011). Contrasting biogeochemistry of nitrogen in the Atlantic and Pacific oxygen minimum zones. *Biogeosciences Discussions*, 8(4), 8001–8039. <https://doi.org/10.5194/bgd-8-8001-2011>

1085 Santoro, A. E., Buchwald, C., McIlvin, M. R., & Casciotti, K. L. (2011). Isotopic Signature of N_2O Produced by Marine Ammonia-Oxidizing Archaea. *Science*, 333, 1282–1285. <https://doi.org/10.1126/science.1208239>

1090 Santoro, A. E., & Casciotti, K. L. (2011). Enrichment and characterization of ammonia-oxidizing archaea from the open ocean: phylogeny, physiology and stable isotope fractionation. *The ISME Journal*, 5(11), 1796–1808. <https://doi.org/10.1038/ismej.2011.58>

1095 Santoro, A. E., Casciotti, K. L., & Francis, C. A. (2010). Activity, abundance and diversity of nitrifying archaea

and bacteria in the central California Current. *Environmental Microbiology*, 12(7), 1989–2006. <https://doi.org/10.1111/j.1462-2920.2010.02205.x>

Santoro, A. E., Dupont, C. L., Richter, R. A., Craig, M. T., Carini, P., McIlvin, M. R., ... Saito, M. A. (2015). Genomic and proteomic characterization of “Candidatus Nitrosopelagicus brevis”: An ammonia-oxidizing archaeon from the open ocean. *Proceedings of the National Academy of Sciences*, 112(4), 1173–1178. <https://doi.org/10.1073/PNAS.1416223112>

Schmidtko, S., Stramma, L., & Visbeck, M. (2017). Decline in global oceanic oxygen content during the past five decades. *Nature*, 542(7641), 335–339. <https://doi.org/10.1038/nature21399>

Schunck, H., Lavik, G., Desai, D. K., Großkopf, T., Kalvelage, T., Löscher, C. R., ... Laroche, J. (2013). Giant hydrogen sulfide plume in the oxygen minimum zone off Peru supports chemolithoautotrophy. *PloS One*, 8(8), e68661. <https://doi.org/10.1371/journal.pone.0068661>

Segata, N., Izard, J., Waldron, L., Gevers, D., Miropolsky, L., Garrett, W. S., & Huttenhower, C. (2011). Metagenomic biomarker discovery and explanation. *Genome Biology*, 12(6), R60. <https://doi.org/10.1186/gb-2011-12-6-r60>

Shoun, H., Fushinobu, S., Jiang, L., Kim, S. W., & Wakagi, T. (2012). Fungal denitrification and nitric oxide reductase cytochrome P450nor. *Philosophical Transactions of the Royal Society B: Biological Sciences*, 367(1593), 1186–1194. <https://doi.org/10.1098/rstb.2011.0335>

Sigman, D. M., Casciotti, K. L., Andreani, M., Barford, C., Galanter, M., & Böhlke, J. K. (2001). A Bacterial Method for the Nitrogen Isotopic Analysis of Nitrate in Seawater and Freshwater. *Analytical Chemistry*, 73, 4145–4153.

Stein, L. Y. (2019). Insights into the physiology of ammonia-oxidizing microorganisms. *Current Opinion in Chemical Biology*, 49, 9–15. <https://doi.org/10.1016/J.CBPA.2018.09.003>

Stewart, F. J., Ulloa, O., & Delong, E. F. (2011). Microbial metatranscriptomics in a permanent marine oxygen minimum zone. *Environmental Microbiology*, 14(1), 23–40. <https://doi.org/10.1111/j.1462-2920.2010.02400.x>

Stewart, F. J., Dalsgaard, T., Young, C. R., Thamdrup, B., Revsbech, N. P., Ulloa, O., ... Delong, E. F. (2012). Experimental incubations elicit profound changes in community transcription in OMZ bacterioplankton. *PloS One*, 7(5), e37118. <https://doi.org/10.1371/journal.pone.0037118>

Stieglmeier, M., Mooshammer, M., Kitzler, B., Wanek, W., Zechmeister-Boltenstern, S., Richter, A., & Schleper, C. (2014). Aerobic nitrous oxide production through N-nitrosating hybrid formation in ammonia-oxidizing archaea. *The ISME Journal*, 8(5), 1135–1146. <https://doi.org/10.1038/ismej.2013.220>

Stramma, L., Bange, H. W., Czeschel, R., Lorenzo, A., & Frank, M. (2013). On the role of mesoscale eddies for the biological productivity and biogeochemistry in the eastern tropical Pacific Ocean off Peru. *Biogeosciences*, 10(11), 7293–7306. <https://doi.org/10.5194/bg-10-7293-2013>

Stramma, Lothar, Johnson, G. C., Sprintall, J., & Mohrholz, V. (2008). Expanding Oxygen-Minimum Zones in the Tropical Oceans. *Science*, 320, 655–659.

Sun, X., Ji, Q., Jayakumar, A., & Ward, B. B. (2017). Dependence of nitrite oxidation on nitrite and oxygen in low-oxygen seawater. *Geophysical Research Letters*, 44(15), 7883–7891. <https://doi.org/10.1002/2017GL074355>

Swan, B. K., Martinez-Garcia, M., Preston, C. M., Sczyrba, A., Woyke, T., Lamy, D., ... Stepanauskas, R. (2011). Potential for chemolithoautotrophy among ubiquitous bacteria lineages in the dark ocean. *Science*, 333(6047), 1296–1300. <https://doi.org/10.1126/science.1203690>

Thamdrup, B., & Dalsgaard, T. (2002). Production of N₂ through Anaerobic Ammonium Oxidation Coupled to Nitrate Reduction in Marine Sediments. *Applied and Environmental Microbiology*, 68(3), 1312–1318. <https://doi.org/10.1128/aem.68.3.1312-1318.2002>

Thomsen, J. K., Geest, T., & Cox, R. P. (1994). Mass Spectrometric Studies of the Effect of pH on the Accumulation of Intermediates in Denitrification by *Paracoccus denitrificans*. *Applied and Environmental Microbiology*, 60(2), 536–541.

Tiano, L., Garcia-Robledo, E., Dalsgaard, T., Devol, A. H., Ward, B. B., Ulloa, O., ... Peter Revsbech, N. (2014). Oxygen distribution and aerobic respiration in the north and south eastern tropical Pacific oxygen minimum zones. *Deep-Sea Research Part I: Oceanographic Research Papers*, 94, 173–183. <https://doi.org/10.1016/j.dsr.2014.10.001>

Torres-Beltrán, M., Mueller, A., Scofield, M., Pachiadaki, M. G., Taylor, C., Tyschenko, K., ... Hallam, S. J. (2019). Sampling and processing methods impact microbial community structure and potential activity in a seasonally anoxic fjord: Saanich inlet, British Columbia. *Frontiers in Marine Science*, 6(MAR), 1–16. <https://doi.org/10.3389/fmars.2019.00132>

Trimmer, M., Chronopoulou, P.-M., Maanoja, S. T., Upstill-Goddard, R. C., Kitidis, V., & Purdy, K. J. (2016). Nitrous oxide as a function of oxygen and archaeal gene abundance in the North Pacific. *Nature Communications*, 7, 13451. <https://doi.org/10.1038/ncomms13451>

Vajrala, N., Martens-Habbena, W., Sayavedra-Soto, L. A., Schauer, A., Bottomeley, P. J., Stahl, D. A., & Arp, D. J. (2013). Hydroxylamine as an intermediate in ammonia oxidation by globally abundant marine archaea. *Proceedings of the National Academy of Sciences*, 110(3), 1006–1011.

https://doi.org/10.1073/pnas.1214272110

1115 Van Der Star, W. R. L., Van De Graaf, M. J., Kartal, B., Picioreanu, C., Jetten, M. S. M., & Van Loosdrecht, M. C. M. (2008). Response of anaerobic ammonium-oxidizing bacteria to hydroxylamine. *Applied and Environmental Microbiology*, 74(14), 4417–4426. <https://doi.org/10.1128/AEM.00042-08>

Wankel, S. D., Ziebis, W., Buchwald, C., Charoenpong, C., De Beer, Di., Dentinger, J., ... Zengler, K. (2017). Evidence for fungal and chemodenitrification based N₂O flux from nitrogen impacted coastal sediments. *Nature Communications*, 8, 1–11. <https://doi.org/10.1038/ncomms15595>

1120 Ward, B. B., Tuit, C. B., Jayakumar, A., Rich, J. J., Moffett, J., & Naqvi, S. W. a. (2008). Organic carbon, and not copper, controls denitrification in oxygen minimum zones of the ocean. *Deep-Sea Research Part I: Oceanographic Research Papers*, 55(12), 1672–1683. <https://doi.org/10.1016/j.dsr.2008.07.005>

Weier, K. L., Doran, J. W., Power, J. F., & Walters, D. T. (1993). Denitrification and the Dinitrogen/Nitrous Oxide Ratio as Affected by Soil Water, Available Carbon, and Nitrate. *Soil Science Society of America Journal*, 57(1), 66. <https://doi.org/10.2136/sssaj1993.03615995005700010013x>

1125 Weigand, M. A., Foriel, J., Barnett, B., Oleynik, S., & Sigman, D. M. (2016). Updates to instrumentation and protocols for isotopic analysis of nitrate by the denitrifier method. *Rapid Communications in Mass Spectrometry*, 30(12), 1365–1383. <https://doi.org/10.1002/rcm.7570>

Wright, J. J., Konwar, K. M., & Hallam, S. J. (2012). Microbial ecology of expanding oxygen minimum zones. *Nature Reviews Microbiology*, 10(6), 381–394. <https://doi.org/10.1038/nrmicro2778>

Wuchter, C., Abbas, B., Coolen, M. J. L., Herfort, L., van Bleijswijk, J., Timmers, P., ... Sinninghe Damsté, J. S. (2006). Archaeal nitrification in the ocean. *Proceedings of the National Academy of Sciences of the United States of America*, 103(33), 12317–12322. <https://doi.org/10.1073/pnas.0600756103>

1130 Yang, S., Gruber, N., Long, M. C., & Vogt, M. (2017). High ENSO driven variability of denitrification and suboxia in the Eastern Pacific Ocean. *Global Biogeochemical Cycles* 31(10) 1470-1487. <https://doi.org/10.1002/2016GB005596>

Yoshida, N. (1988). ¹⁵N-depleted N₂O as a product of nitrification. *Nature*, 335(6190), 528–529. <https://doi.org/10.1038/335528a0>

1135 Zhou, Z., Takaya, N., Sakairi, M. A. C., & Shoun, H. (2001). Oxygen requirement for denitrification by the fungus *Fusarium oxysporum*. *Archives of Microbiology*, 175(1), 19–25. <https://doi.org/10.1007/s002030000231>

Zhu-Barker, X., Cavazos, A. R., Ostrom, N. E., Horwath, W. R., & Glass, J. B. (2015). The importance of abiotic reactions for nitrous oxide production. *Biogeochemistry*, 126(3), 251–267. <https://doi.org/10.1007/s10533-015-0166-4>

1140 Zumft, W. G. (1997). Cell biology and molecular basis of denitrification. *Microbiology and Molecular Biology Reviews*, 61(4), 533–616.

Tables

1150

Table 1: Overview of characteristics of samples. bd - below detection limit of Winkler method and seabird sensor ($2 \mu\text{mol L}^{-1}$), x - analysis includes qPCR and microarray with qPCR products, x* - only qPCR, no microarray

ID	Stat #	Coordinates/position	bottom depth (m)	sampling depth (m)	water column feature	Tem. (°C)	Sal.	O_2 (μM) seabird	NO_3^- (μM)	NO_2^- (μM)	NH_4^+ (μM)	^{15}N incubation	Tracer added	nirS	amoA
S2	882	10.95W 78.56N	1075	352	anoxic core	11.4	34.82	bd	32.51	0.68	0.01	depth profile	NH_4^+ , NO_2^- , NO_3^-	x	x
S1	882		1075	299	below interface	12.1	34.86	bd	30.21	0.52	0.00	depth profile	NH_4^+ , NO_2^- , NO_3^-	x	x
S3	882		1075	259	oxic-anoxic interface	13.0	34.92	bd	29.39	1.63	0.01	depth profile	NH_4^+ , NO_2^- , NO_3^-	x	x
S4	882		1075	219	above interface	13.7	34.96	6.06	31.65	0.13	0.01	depth profile	NH_4^+ , NO_2^- , NO_3^-	x	x
S5	882		1075	74	oxycline	15.4	35.05	15.04	30.00	0.02	0.00	depth profile	NH_4^+ , NO_2^- , NO_3^-	x	x
S6	883	10.78W 78.27N	305	305	anoxic core	12.2	34.87	bd	27.27	1.72	0	depth profile	NH_4^+ , NO_2^- , NO_3^-	x	x
S7	883		305	268	below interface	12.8	34.91	bd	26.61	2.05	0	depth profile	NH_4^+ , NO_2^- , NO_3^-	x	x
S8	883		305	250	oxic-anoxic interface	13.1	34.92	bd	28.06	1.66	0	depth profile	NH_4^+ , NO_2^- , NO_3^-	x	x
S9	883		305	189	above interface	13.8	34.97	bd	30.47	0.00	0	depth profile	NH_4^+ , NO_2^- , NO_3^-	x	x
S10	883		305	28	oxycline	16.4	35.09	30.06	26.81	0.04	0	depth profile	NH_4^+ , NO_2^- , NO_3^-	x	x
S19	892	12.41W 77.81N/	1099	144	below oxic-anoxic interface	13.51	34.91	bd	19.01	3.69	0.13	O_2 manipulation	NH_4^+ , NO_2^- , NO_3^-	x	x
S11	894	12.32W 77.62N/	502	120	oxic-anoxic interface	14.21	34.98	bd	28.92	0.01	0.00	O_2 manipulation	NH_4^+ , NO_2^- , NO_3^-	x	x
S12	904	13.99W 76.66N	560	179	below interface	13.46	34.94	bd	25.54	1.25	0.00	POM addition (from 898)	NO_2^- , NO_3^-	x	x*
S13	904		560	124	oxic-anoxic interface	14.40	35.00	bd	27.57	0.09	0.00	POM addition (from 898)	NO_2^- , NO_3^-	x	x*
S14	906	14.28W 77.17N	4761	149	below interface	13.70	34.96	bd	25.80	0.90	0.04	POM addition (from 904)	NO_2^- , NO_3^-	x	x*
S20	906		4761	92	oxic-anoxic interface	14.50	35.00	bd	20.03	3.87	0.33	POM addition (from 904)	NO_2^- , NO_3^-	x	x*
S15	907	15.43W 75.43N	800	130	below interface	14.21	34.98	bd	14.63	5.23	0.03	POM addition (from 904)	NO_2^- , NO_3^-	x	x
S16	907		800	9.9	surface	17.82	35.13	208.3	16.09	0.99	0.16	POM addition (from 904)	NO_2^- , NO_3^-	x	x
S17	912	15.86W 76.11N	3680	90	below interface	15.09	35.03	bd	19.38	2.85	0.03	POM addition (from 906)	NO_2^- , NO_3^-	x	x
S18	912		3680	5	surface	18.05	35.18	206.0	8.31	0.47	0.12	POM addition (from 906)	NO_2^- , NO_3^-	x	x
S21	917	14.78W 78.04N/	4128	140	Interface	13.1	34.86	bd	17.3	3.9	0.0	POM addition (from 906)	NO_2^- , NO_3^-	x	x*

Table 2: Quality (N/C), quantity (Addition $\mu\text{mol L}^{-1}$) and origin (station and depth) of added, autoclaved and non-autoclaved particulate organic matter (POM) and increase in NH_4^+ concentration after autoclaving.

POM	Feature	Station	Depth (m)	Addition ($\mu\text{mol L}^{-1}$)	N/C of autoclaved POM	N/C of non- autoclaved POM	NH_4^+ (μM) after autoclaving
POM 1	mixed layer depth	898	60	0.55	0.10	0.15	0.7
		904	20	0.17	0.09	0.17	1.56
		906	50	0.48	0.07	0.11	0.57
POM 2	oxycline	898	100	1.37	0.06	0.13	0.85
		904	50	0.38	0.09	0.12	0.46
		906	100	0.44	0.08	0.10	0.55
POM 3	anoxic zone	898	300	0.43	0.09	0.10	0.15
		904	150	0.19	0.10	0.10	0.20

Figure Legends:

1160

Figure 1: Study area with the distribution of near-surface chlorophyll concentrations (monthly averaged for June 2017) from MODIS satellite obtained from the NASA Ocean Color Web site at 4-km resolution. Study site showing transect and station numbers, in the Eastern Tropical South Pacific during cruise M138.

1165

Figure 2: Depth profiles of O₂, nutrients and N₂O in the upper 400 m for all stations. Panel numbers 1 - 4) refer to the transect numbers.

1170

Figure 3: (I) Profiles of AO, (a, e, I), N₂O production rates from NH₄⁺ (b, f, j), archaeal *amoA* gene (c, g, k) and transcript copy numbers mL⁻¹ (d, h, l). (II) Profiles of NO₃⁻ reduction rates (a, f, k, o), N₂O production rates from NO₃⁻ (b, g, l, p) and NO₂⁻ (c, h, m, q) and *nirS* gene (d, I, n, r) and transcript copy numbers mL⁻¹ (e, j, m, s). In (I) and (II), the panel numbers 1 – 4 correspond to transect numbers. Negative values on the y-axis represent shallower, oxic depths and the positive values represent deeper, anoxic depth (0 = interface). Shaded area indicates the anoxic zone. Note different scale for N₂O production rates.

1175

Figure 4: O₂ dependence of N₂O production rates from NH₄⁺ (a, d), NO₂⁻ (b, e) and NO₃⁻ (c, f). Upper panel (a-c) is N₂O production along natural O₂ gradient from all stations. Figure 4 (b, c) are additionally zoomed in to oxygen concentrations below 5 μmol L⁻¹. Lower panel (d-f) is N₂O production in manipulated O₂ experiments with water from oxic - anoxic interface from slope station 892 (S11, 0 μmol L⁻¹ O₂, 145m) and shelf station 894 (S19, 0 μmol L⁻¹, 120 m). Note different scale for N₂O production rates from NH₄⁺. Vertical error bars represent ± Standard error (n = 5 per time course). Horizontal error bars represent ± Standard error of measured O₂ over the time of incubations (n = 6).

1180

Figure 5: O₂ dependency of hybrid N₂O formation from NH₄⁺ (a, c) and NO₂⁻ (b, d) along the natural O₂ gradient (a, b) and for the O₂ manipulations (c, d) from sample S11 (0 μmol L⁻¹ O₂, 145m) and S19 (894, 0 μmol L⁻¹, 120 m)

1185

Figure 6: Yields (%) of N₂O production during NH₄⁺ oxidation (a, c) and during NO₃⁻ reduction (b, d) along the natural O₂ gradient (a, b) and for the O₂ manipulations (c, d) from sample S11 (892, 0 μmol L⁻¹ O₂, 145m) and S19 (894, 0 μmol L⁻¹, 120 m). Error bars present ± SD calculated as error propagation.

1190

Figure 7: Bar plots of N₂O production after additions of autoclaved suspended and sinking particles >50 μm (See Table 2). POM1 = mixed layer depth, POM2 = oxycline, POM3 = ODZ. Error Bars represent ± SE of linear regression. * indicates significant difference to control rate (p < 0.05)

Figure 8: Stacked bar plot of community composition of AOA *amoA* archetypes (a, b) and *nirS* archetypes (c, d). Only archetypes over 1% contribution are shown. (a, c) total community composition (DNA). (b, d) active community composition (cDNA).

Figure 9: Scheme illustrating the possible reactions for hybrid N₂O formation. The ellipse represents an AOA cell.

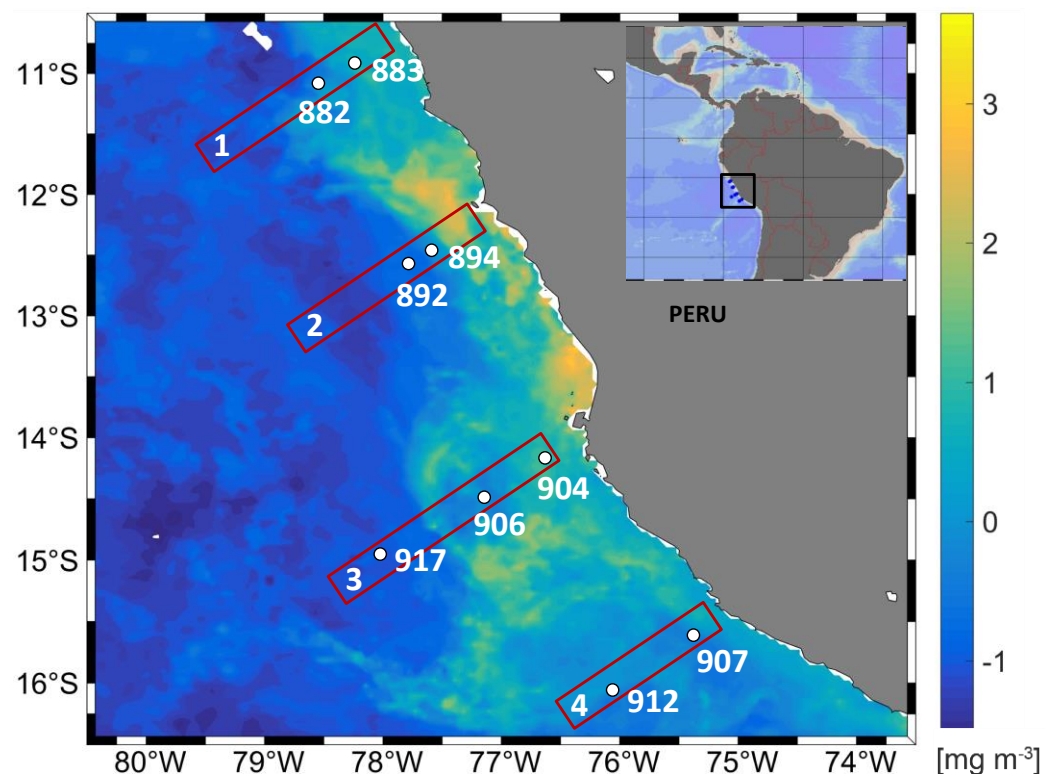


Figure 1

1195

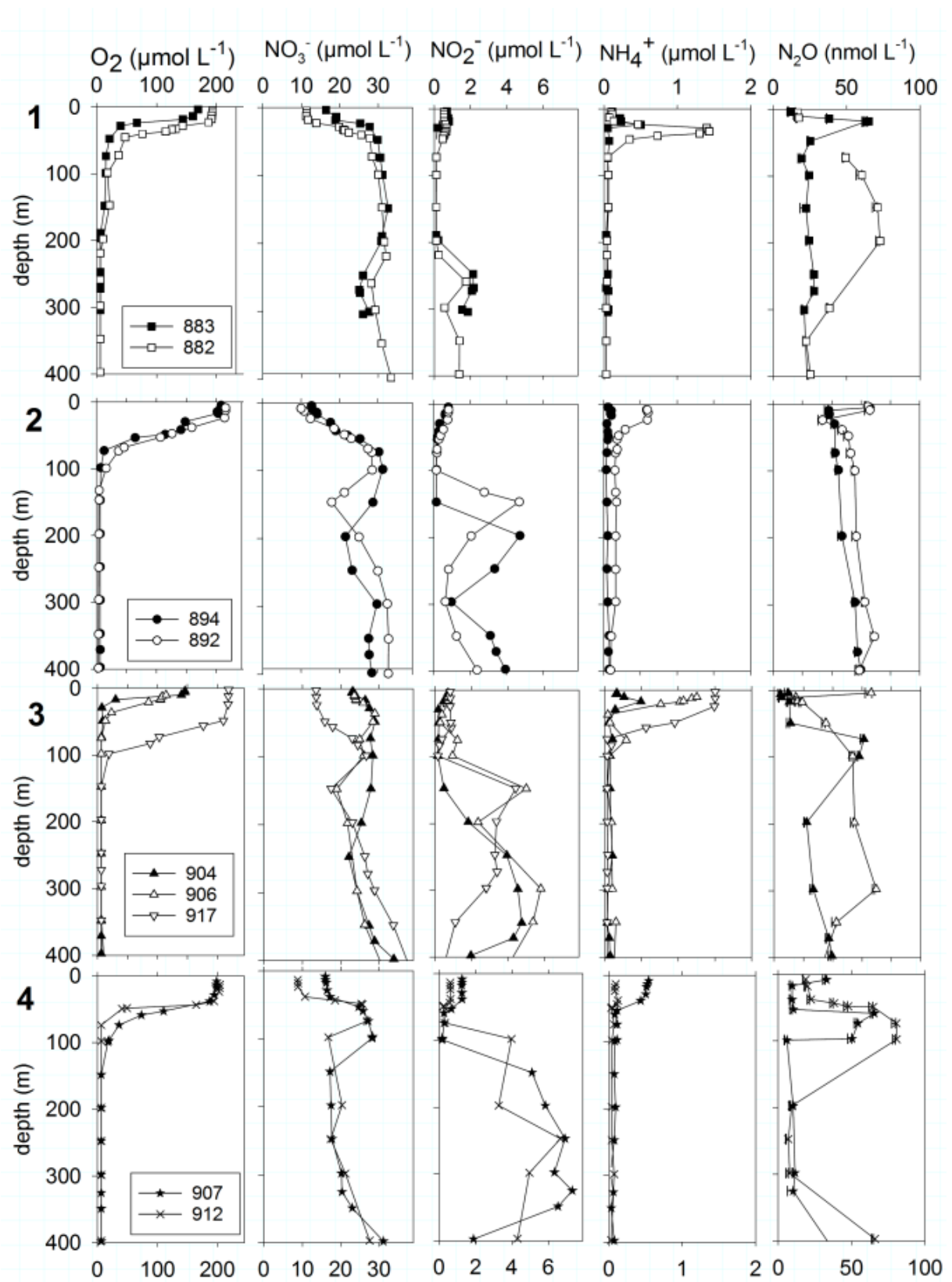


Figure 2

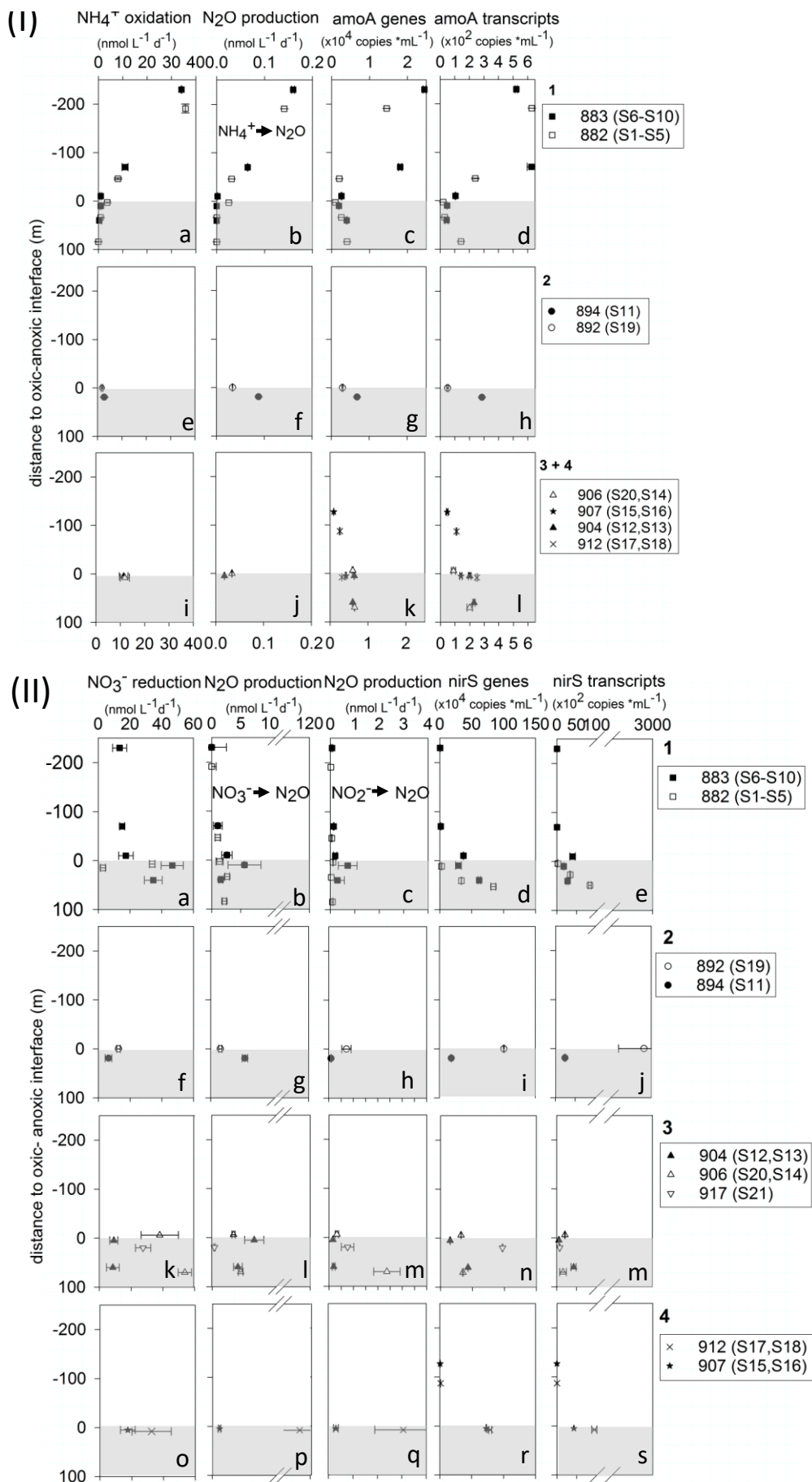
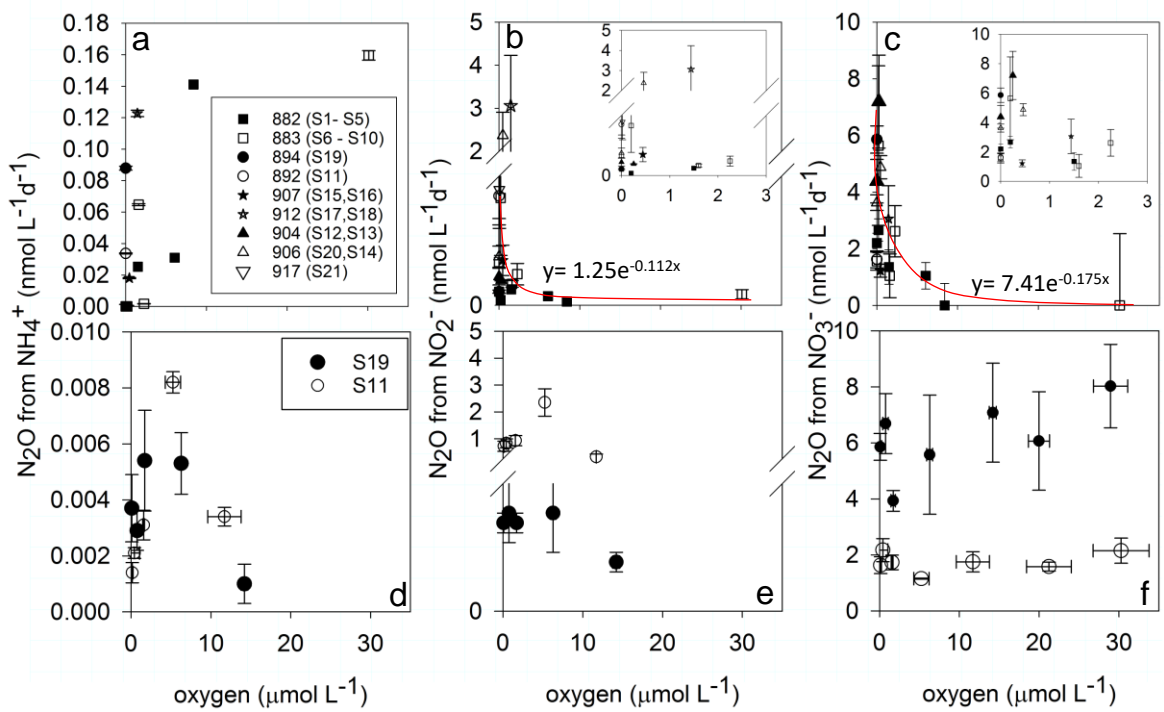


Figure 3



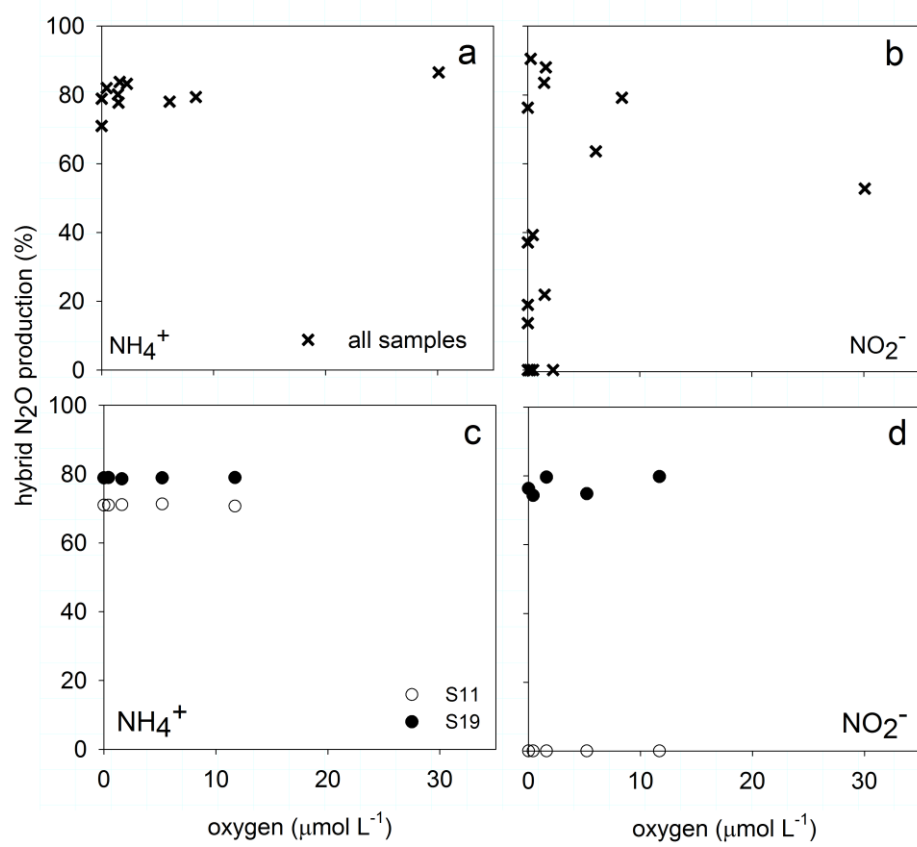
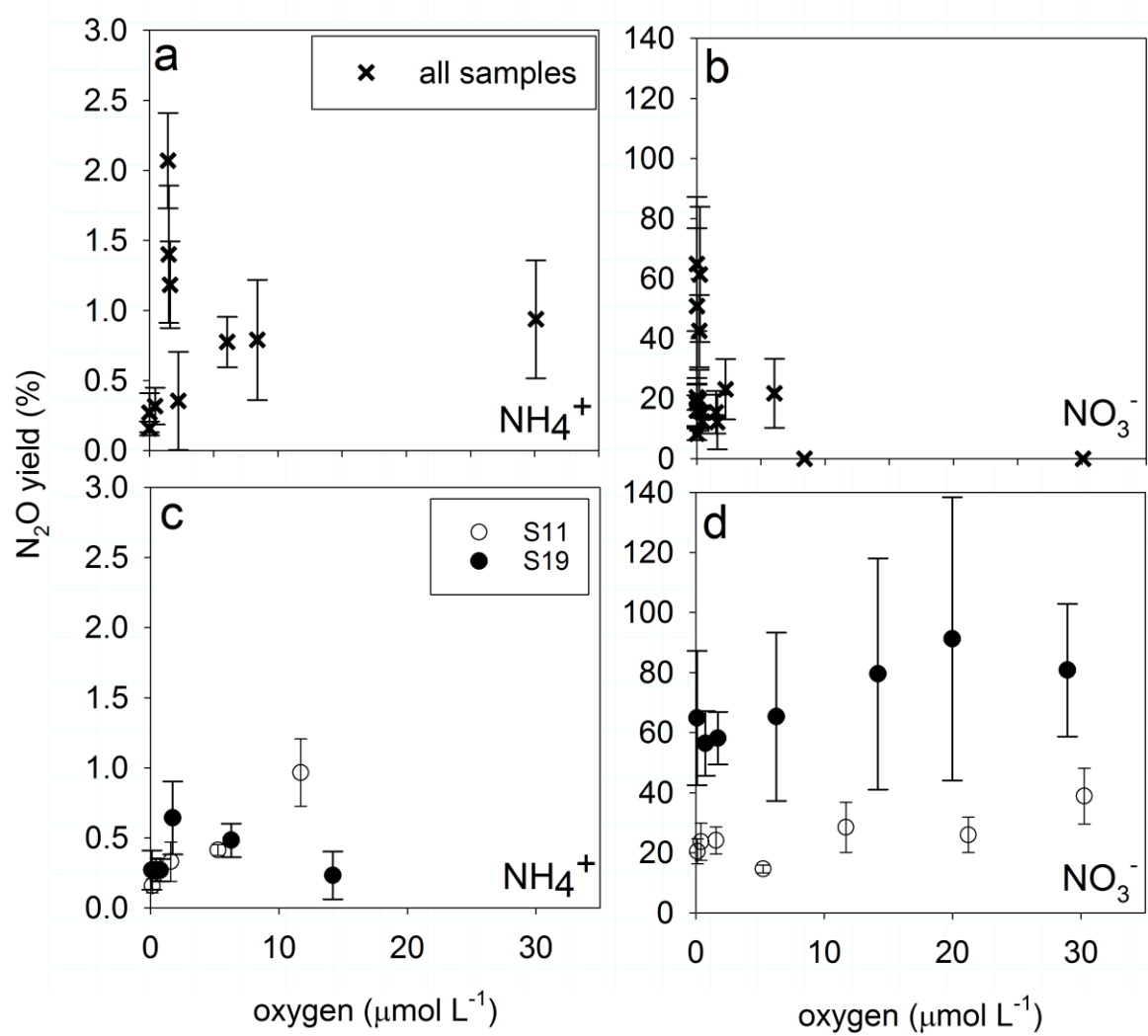


Figure 5

1205



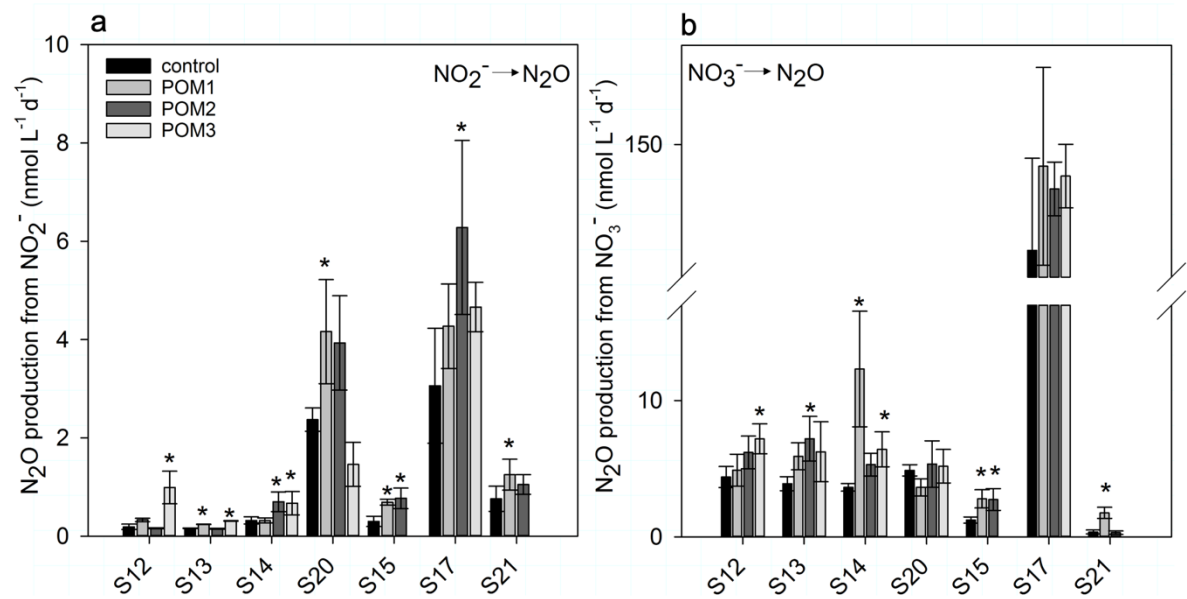
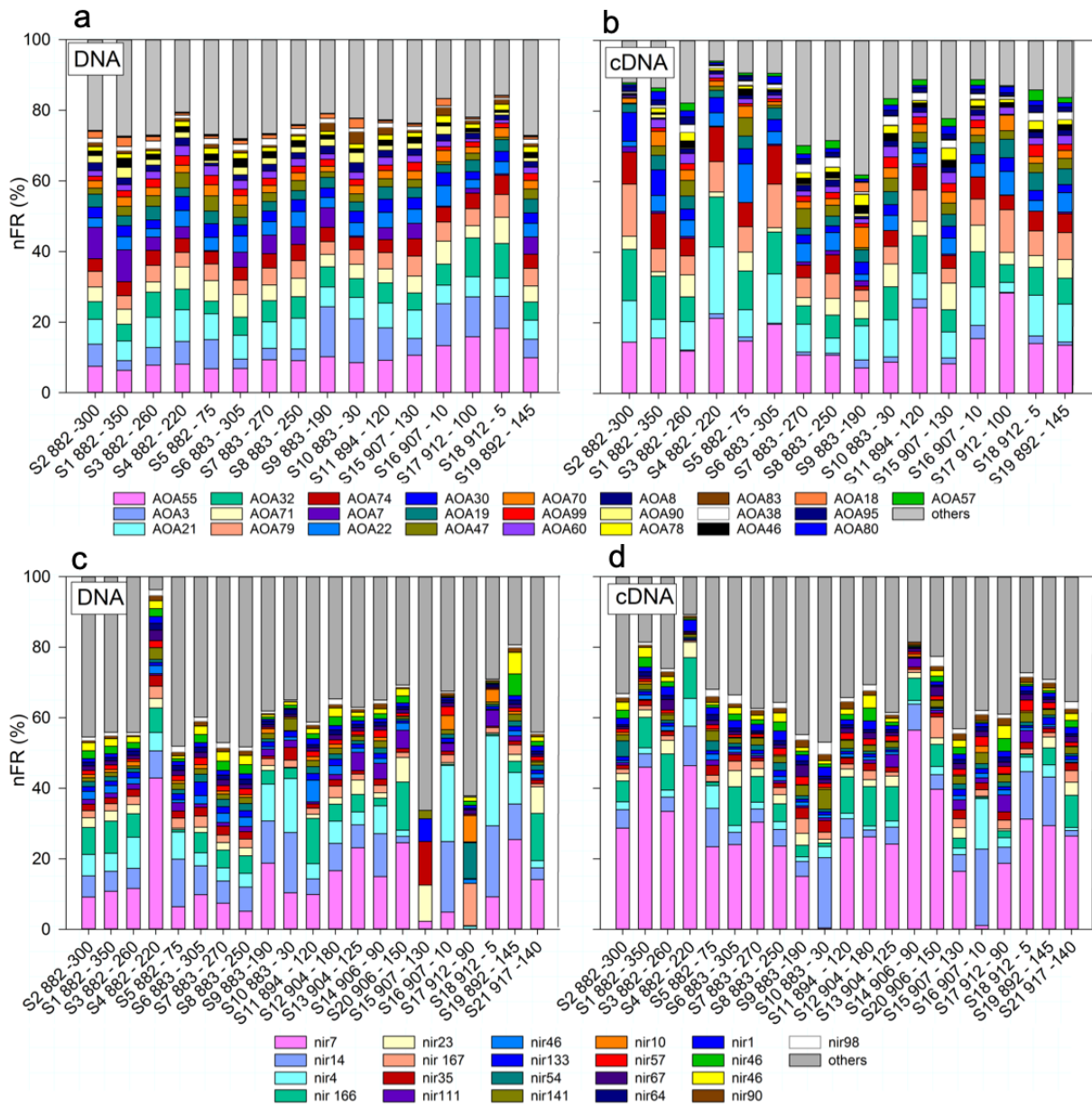
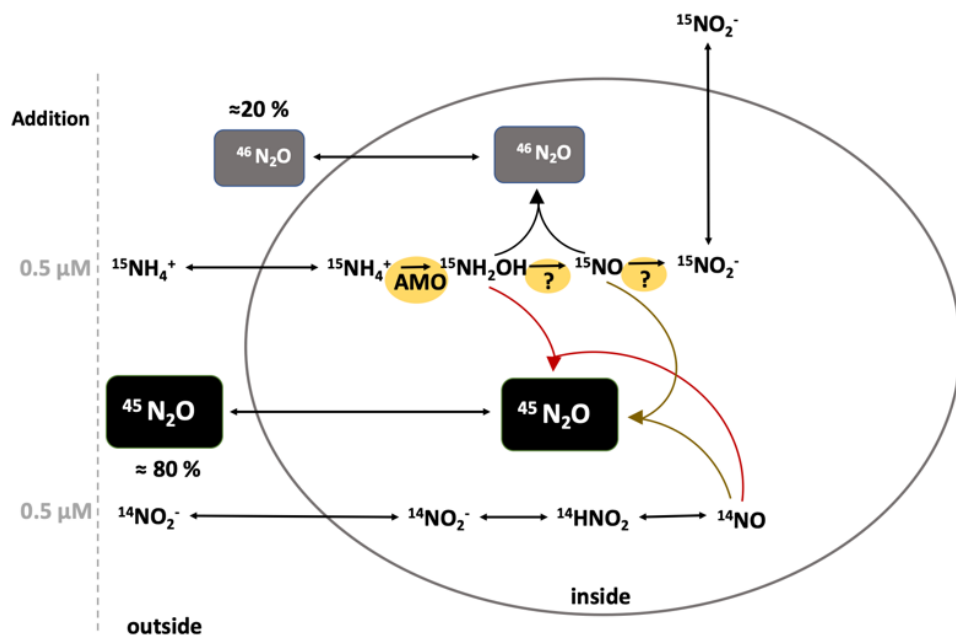


Figure 7



1215 **Figure 8**



1220 **Figure 9**